

Towards a 3D printed patient clone: Application to the effect of aortic regurgitation on the flow in the left ventricle

Max Lavigne

A Thesis

In the department of

Mechanical, Industrial and Aerospace Engineering

Presented in partial fulfillment of the requirements

for the degree of Master of Applied Science (Mechanical Engineering) at

Concordia University

Montreal, Quebec, Canada

June 2020

© Max Lavigne, 2020

CONCORDIA UNIVERSITY
School of Graduate Studies

This is to certify that the thesis prepared

By: **Max Lavigne**

Entitled: **“Towards a 3D printed patient clone: Application to the effect of aortic regurgitation on the flow in the left ventricle”**

and submitted in partial fulfillment of the requirements for the degree of

Master of Applied Science (Mechanical Engineering)

Complies with the regulations of the University and meets the accepted standards with respect to originality and quality

Signed by the Final examining committee:

_____	Chair
Dr. Charles Basenga Kiyanda	
_____	Examiner
Dr. Rolf Wuthrich	
_____	Thesis Supervisor(s)
Dr. Lyes Kadem	

Dr. Julio Garcia	

Approved by

Dr. Mamoun Medraj, MAsc Graduate Program Director

Dr. Mourad Debabbi, Dean
Gina Cody School of Engineering & Computer Science

Date: July 22, 2020

Abstract

Towards a 3D printed patient clone: Application to the effect of aortic regurgitation on the flow in the left ventricle

Max Lavigne

Heart disease is the leading cause of death in the world. Amongst the many cardiovascular diseases, heart valve failure is a common reoccurrence. Patient safety has risen to being a top priority focus for every field of medicine therefore heart simulators are implemented and expected to contribute immensely to the medical training of physicians, medical device testing and the study of cardiovascular fluid dynamics. Common methods to studying cardiovascular fluid dynamics have been the use of Doppler echocardiography or 2D plane analysis using particle image velocimetry. The objective of this thesis is to design an innovated 3D printed heart simulator which is completely mobile and M.R.I. (magnetic resonance imaging)-compatible which can obtain results that are not possible with present methods. The 3D printed heart simulator created for this dissertation was named the MaxTron system. Among the many heart diseases that could be modeled with the system, aortic regurgitation was chosen to demonstrate one of its many capabilities. Simulation was controlled through guided wires entering the 3D printed representation of the left side of a male patient's heart. Each leaflet of the aortic heart valve could be independently controlled to represent different severities of the disease. Results demonstrate the accuracy of 4D flow readings and the versatility of the system. Vortex formation and particle pathlines formed by aortic regurgitation and mitral inflow interaction can be observed from any angle or plane during both diastolic and systolic phases. Lifelike heart valves perform better for M.R.I. experiments when compared to both mechanical and bio-prosthetic heart valves that contain metal components which are less M.R.I.-compatible.

Acknowledgments

This project is an evolution of great ideas and contributions guided by Dr. Lyes Kadem. For his guidance in the project and all his wise advice, I am deeply indebted. Co-supervisor Dr. Julio Garcia made M.R.I. experimentation possible and his skills were essential to the project's success. Previous L.C.F.D. Capstone teams that led the progress through the early iterations of the project equally share all merit to increasing patient safety, especially Alexis Arévalo Tejada, Ramit Singh, Kevin Gandhi, Zachary Zoldan, Sebouh Akhikian, Nicholas Bonomo, Constantinos Danias, Kyo, Subi Fox, Tabitha Jaramillo, Sholom Shuchat and Jana Ghalayini. Guidance and collaborations with Dr. Giuseppe Di Labbio PhD eng, Ghassan Maraouch BAsC Eng, Ahmed Darwish MAsc eng, Maziar Sargordi MAsc Eng and Amanda Mikhail MAsc Eng. along with other colleagues at the L.C.F.D. were truly memorable and deserve honorable mention. Photographic contributions by Benjamin Lavigne from Bling Consultants Inc. were truly appreciated. Efforts by Sameera Rana were imperative to the success of this study along with the love and support that was received from my friends and family. This thesis is dedicated to my son Devon Toki Rana Lavigne, you can achieve anything that you set your mind to.

Lastly, I would like to extend a special thank you to those who took the time to review and grade this thesis submission.

Thank you all very much!

Table of Contents

Table of Figures	vii
Nomenclature.....	viii
1 Introduction.....	1
1.1.1. The Heart	1
1.1.2. Heart Valves	2
1.1.3. Intra-cardiac Pressure	4
1.1.4. Heart Disease	5
1.1.5. Heart Valve Disease	6
1.1.6. Aortic Regurgitation	6
1.2.1. Cardiovascular Research	8
1.2.2. Cardiovascular Device Testing.....	8
1.2.3. Cardiovascular Medical Training	11
1.2.4. Cardiovascular Fluid Dynamics	12
1.3.1. Thesis Objective	13
2 Literature Review	15
2.1.1. Cardiovascular <i>In vivo</i> Studies	15
2.1.2. Cardiovascular <i>In vitro</i> Studies	17
2.1.3. Cardiovascular Research of Today	20
2.2.1. Cardiovascular Simulators.....	22
2.2.2. 3D Printing-based Heart Simulator	23
3 Methodology.....	25
3.1.1. State of the Art.....	25
3.1.2. The MaxTron System	25
3.1.2. Simulator Casing Considerations	28
3.1.3. Heart Components	30
3.1.4. Screwclamps	33
3.1.5. Heart Valves	34
3.1.6. Heart Support Structure	35
3.1.7. Hydraulic Activation System.....	36
3.1.8. Aortic Regurgitation	38
3.1.9. Mitral Valve Orientation.....	39

3.2.1. Magnetic Resonance Imaging.....	40
3.2.2. Molecular Nuclei Magnetisation	42
3.2.3. M.R.I. Acquisition Steps	48
3.2.4. Repetition Time	53
3.2.5. Flow Velocity Mapping.....	55
3.3.1. M.R.I. Parameters for the MaxTron System.....	56
4 Results.....	58
4.1.1. Introduction.....	58
4.1.2. M.R.I. Compatibility.....	61
4.1.3. M.R.I. 3-Dimensional Results	62
4.1.4. 2-Dimensional Results.....	64
4.1.5. Aortic Regurgitation Simulation.....	68
4.1.6. Mitral Valve Orientation.....	72
5 Conclusion	75
5.1.1. Discussion.....	75
5.1.2. Limitations.....	78
● References.....	79
● Appendix 1 Aortic Regurgitation Setup Selections.....	86
● Appendix 2 Supervisor Information	87
● Appendix 3 The MaxTron System	88
● Appendix 4 System Maintenance	88
● Appendix 5 Experimentation Iterations.....	89

Table of Figures

Figure 1.1: Adaptation of heart components and cycles.....	3
Figure 1.2: Adaptation of Wigger’s diagram.....	5
Figure 1.3: Adaptation of aortic regurgitation.....	7
Figure 1.4: Adaptation of both a tissue heart valve and mechanical heart valve	9
Figure 2.1: Adaptation of the Bellhouse experiment model of left ventricular flow	18
Figure 2.2: ViVitro Labs Endovascular Simulator.....	23
Figure 3.1: Schematic overview of the left side of the MaxTron system.....	27
Figure 3.2: The MaxTron System.....	27
Figure 3.3: Heart valves used during project iterations.....	34
Figure 3.4: Assembly of valve placement between the left ventricle and the left atrium clamped together using a custom made Screwclamp.....	35
Figure 3.5: Heart Support Structure.....	36
Figure 3.6: Aortic regurgitation setup	39
Figure 3.7: Adaptation of the x, y and z gradient coils, integral rf transmitter body coils and the main magnet coils which are used to make M.R.I. acquisitions possible	40
Figure 3.8: Adaptation of the magnetic field surrounding an M.R.I. scanner.....	41
Figure 3.9: Adaptation of the net magnetisation <i>M₀</i> equilibrium which is aligned with the z-axis	43
Figure 3.10: Adaptation of T1 relaxation after 90° Rf pulse of the <i>M_z</i> component	45
Figure 3.11: Adaptation of the transverse component relaxation after 90° Rf pulse	46
Figure 3.12: Contrast obtained in M.R.I. results of the simulator’s left ventricle.....	47
Figure 3.13: Adaptation of step 1 in M.R.I. acquisition.....	49
Figure 3.14: Adaptation of step 2 and 3 of M.R.I. acquisition.....	51
Figure 3.15: Adaptation of the pulse sequence diagram that shows the timing of the Rf and gradient pulses	52
Figure 3.16: Adaptation of phase encoding steps and repetition time.....	54
Figure 3.17: The system within the M.R.I. scanner.....	56
Figure 4.1: Pressure waveforms for both the aorta and left ventricle.....	59
Figure 4.2: Pressure readings for both the pulmonary artery and right ventricle	60
Figure 4.3: Differences in signal reception during acquisitions.....	62
Figure 4.4: Three-dimensional pathline results from M.R.I. acquisitions.....	63
Figure 4.5: M.R.I. acquisition results of a healthy patient simulated case	65
Figure 4.6: Mitral and aortic view of M.R.I. results of a normal patient simulated case.....	67
Figure 4.7: M.R.I. acquisitions of a mild aortic regurgitation simulation.....	69
Figure 4.8: Mitral and aortic view of M.R.I. acquisition results of mild aortic regurgitation simulation	70
Figure 4.9: M.R.I. acquisition results of severe aortic regurgitation simulation	71
Figure 4.10: Mitral orientation change M.R.I. acquisition results for severe aortic regurgitation simulation	73
Figure 5.1: Adaptation of the theoretical placement of soft robotics inside heart component walls enabling realistic compression of the heart	77

Nomenclature

3D	Three Dimensional
ABS	Acrylonitrile Butadiene Styrene
AI	Artificial intelligence
bpm	Beats per minute
cc	Cubic Centimeter
CT	Computerized Tomography
ECG	Electrocardiogram
FDA	Food and Drug Administration
FID	Free Induced Decay
FOV	Field Of View
FSI	Fluid Structure Interaction
LCFD	Laboratory of Cardiovascular Fluid Dynamics
m	Meter
MHz	Megahertz
mL	Millilitre
mmHg	Millimeters of Mercury
MRI	Magnetic Resonance Imaging
ms	Milli-Second
mT	Milli-Tesla
N	Newtons
PIV	Particle Image Velocimetry
PLA	Polylactic Acid
PVC	Polyvinyl Chloride
Rf	Radio Frequency
ROA	Regurgitant Orifice Area
s	Second
STL	Stereolithography
T	Tesla
TE	Echo Time
TR	Repetition time
USA	United States of America
VENC	Velocity Encoding

Page left intentionally blank

Chapter 1

1 Introduction

1.1.1. The Heart

Pulsatile hemodynamic circulation is made possible due to synchronized muscle contractions within the organ known as the heart. The controlled relaxation and contraction of four separate heart chambers in collaboration with four one-way valves between these chambers are beautifully orchestrated in a sequence that permits one-directional flow. The cardiovascular circulatory system provides a means for blood to circulate in order to transport nutrients to and from the body. Blood cells that travel through our lungs exchange oxygen and carbon dioxide, while other cells traveling through intestines collect other essential nutrients. The complete cycle is responsible for a healthy body and immune system. The human heart is comprised of two halves each consisting of their own atrium and ventricle. The cardiac cycle is divided into two separate phases, diastole which occurs during the filling phase of the ventricles, and systole which occurs during the ejection phase of the ventricles. During diastole, the myocardial tissues that make up the ventricle walls relax allowing the volume to expand while refilling with blood [1] [2]. An electrical signal which is delivered through the sinoatrial and atrioventricular nodes at synchronized intervals activates the systolic cycle which is the contraction of myocardial tissues within the atrium and ventricle walls, thus reducing the volume and ejecting the blood flow in a specific trajectory. This process involves specific vortex formations which optimize blood circulation and blood mixture

with the least damage brought upon the blood cells. The direction of the flow is made possible by the heart valves between each chamber [1] [2].

1.1.2. Heart Valves

Atrioventricular valves include heart valves separating atriums and ventricles. The right side atrioventricular valve is known as the tricuspid valve because it has three leaflets whereas the left side atrioventricular valve is known as the mitral valve and consists of only two leaflets. Semilunar valves include heart valves that separate the ventricle from major arteries. The right side semilunar valve is known as the pulmonary valve and separates the right ventricle from the pulmonary artery. The left side semilunar valve is known as the aortic valve and separates the left ventricle from the aorta [1] [2]. The location of the valves and their role in the cardiac cycle can be observed in figure 1.1 [3].

During the diastolic cycle the right ventricle will be filled from the right atrium through the opened tricuspid valve and the left ventricle will be filled from the left atrium through the opened mitral valve. During this cycle the pulmonary and aortic valves are closed and the efficiency of the entire cycle relies heavily on the ability of the heart valves to resist backward flow. When this phase is completed, both atrioventricular valves close due to the reverse pressure caused by the contracting ventricles which directs the flow towards the semi-lunar valves that are now opened. The right ventricle ejects flow through the pulmonary valve into the pulmonary artery which directs the deoxygenated blood towards the lungs. The left ventricle ejects flow through the aortic valve into the aorta bringing oxygenated and nutrient rich blood towards the rest of the body [1] [2].

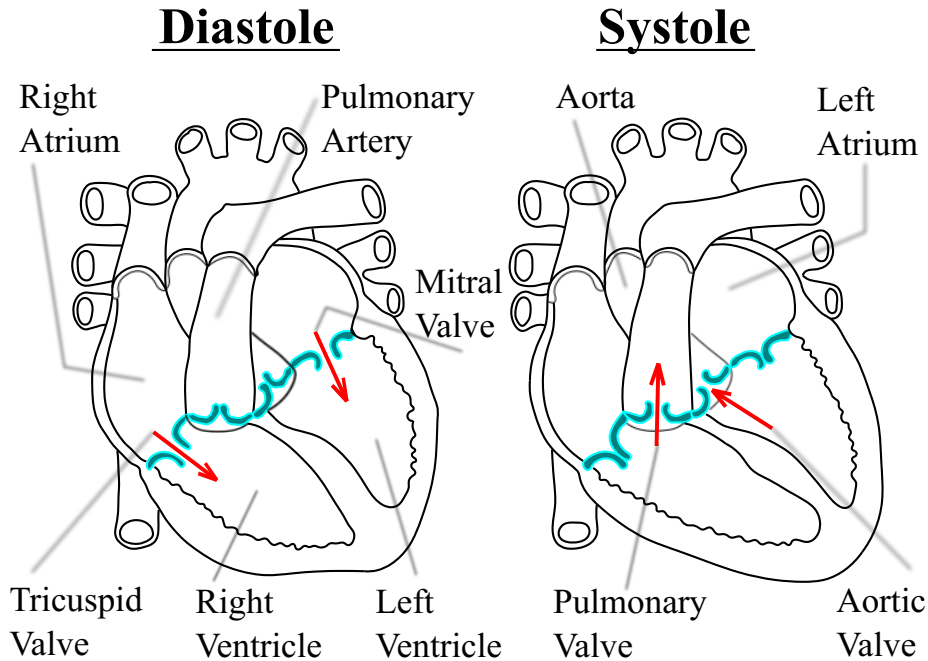


Figure 1.1: Adaptation of heart components and cycles. Modified from image found on the “Texas Heart Institute” website [3]

There are prosthetic replacements available on the market meant to replace diseased or malfunctioning heart valves. There are many types of cardiac valve substitutes that can be implanted into a patient. Although these replacement valves allow patients to continue living, valve life expectancies vary along with patient compatibility. There are many potential side effects implicated with prosthetic heart valves to varying degrees. A few examples include thrombosis (blood clotting), inefficient hemodynamic performance and blood cell damage [4]. The study of heart valve functionality to improve prosthetic heart valve designs is commonly studied through *in vitro* methods [5], which refers to experiments performed on a model replicating an anatomy of interest and not on a living patient.

1.1.3. Intra-cardiac Pressure

The opening and closing of heart valves are mostly controlled by the pressure differences created between chambers and arteries. During diastole, the ventricles are relaxed which lowers the pressure within the ventricles allowing higher inflow pressures to open the tricuspid and mitral valves. Due to their orientation, the pulmonary and aortic valves remain closed till the end of diastole. When the ventricles are filled and systole begins, the pressure difference created by the contracting ventricles accomplishes two things. First, the tricuspid and mitral valves are closed. Secondly, the pulmonary and aortic valves are opened [1] [2]. The complete cycle is a choreographed series of pressure differences and valve functionality which permits hemodynamic circulation throughout the body. Pressure waveforms are of particular importance in cardiovascular research because they can quantifiably assist in the identification of cardiovascular disease severity [1]. Figure 1.2, commonly known as Wigger's diagram, demonstrates the pressure waveforms created by the left side of a healthy heart. Whenever a patient's pressure waveforms deviate from their expected shape, this can be cause for further investigation. Peaks of this waveform coincide with ventricle contraction, or ejection phase at 120 mmHg. The peak of the smaller wave formed shortly after is known as the E wave. It coincides with the rapid filling or inflow phase. Atrial systole is known as the A wave and segmentation is depicted in Wigger's diagram [6].

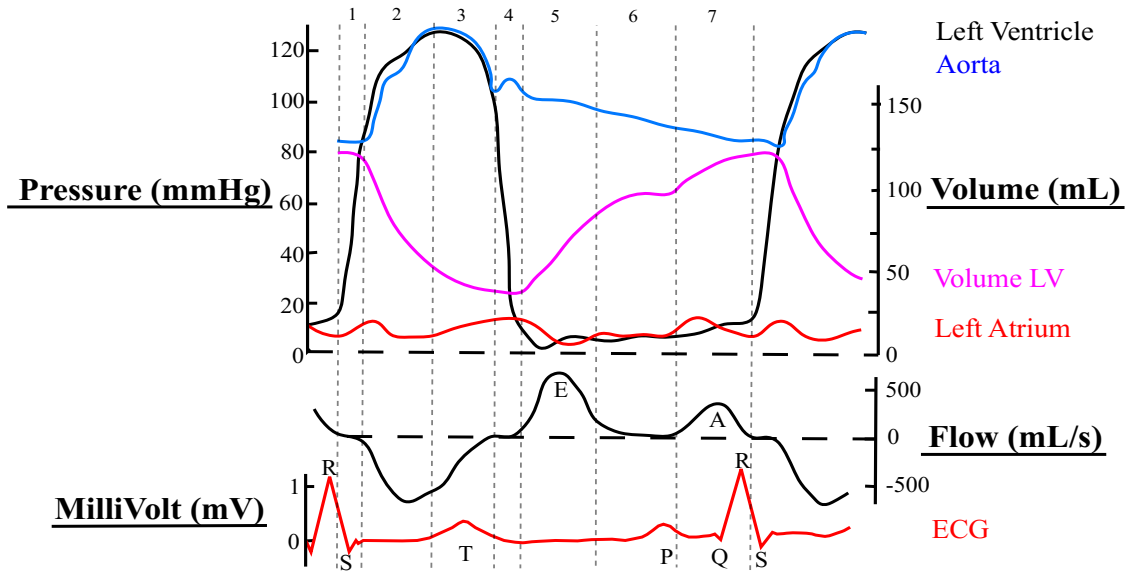


Figure 1.2: Adaptation of Wigger’s diagram. Sections 2 and 3 represent the systolic peak and sections 5, 6 and 7 represent the diastolic phase. Modified from image found in the “Advances in Physiology Education” journal [6]

1.1.4. Heart Disease

The World Health Organisation recognizes cardiovascular disease as the global number one cause of death that is responsible for taking an average of 18 million lives per year [7]. In Canada, it is estimated that cardiovascular disease is responsible for one third of all deaths of the Canadian population and represents 16% of all hospitalizations, not to mention costing the Canadian economy approximately 22\$ billion dollars a year [8]. As the threat continues to escalate, continued efforts towards research and prevention are crucial to finding solutions, including developing new tools which can allow for better understanding of cardiovascular disease and the development of medical devices.

1.1.5. Heart Valve Disease

Aortic and mitral valve replacement surgeries are the most commonly performed amongst heart valve surgeries [9] and valve replacement is the second most common reason for heart surgeries [4]. Proper circulation relies heavily on the functionality of heart valves which depends on the health of the valve's leaflets. Calcification is commonly accumulated upon the leaflets, impeding them from either opening or closing completely, which can eventually lead to certain cardiovascular complications [10]. When heart valves function inefficiently, common associated pathologies are known as stenosis and regurgitation [4]. This dissertation shall focus on aortic regurgitation which occurs when blood leaks back through the valve when the valve is incapable of closing completely [1]. Defective valves cause circulatory dysfunction which can eventually lead to cardiac arrest. To prevent this, the remedy is surgery where a heart valve can either be repaired or replaced. Some medical procedure methods are proven to work better than others and can be better suited for a specific patient therefore careful planning and preventative measures must be taken [1]. All four heart valves are prone to such diseases and represent a very challenging surgery to perform [4].

1.1.6. Aortic Regurgitation

Aortic regurgitation is a cardiovascular defect wherein the aortic valve does not close completely during diastole and allows a regurgitating jet to flow backward into the left ventricle. Studies estimated that 13% of men and 8.5% of women from a sample

population group were suffering from different severities of aortic regurgitation [11]. Aortic regurgitation worsens over time and can lead to multiple potential side effects. Studies have proven that the regurgitating jet from the aorta does interfere with mitral inflow causing flow disturbances [12]. Stagnant blood that spends more time in the ventricle than expected can lead to thrombi, which is the coagulation of blood [13]. Figure 1.3 demonstrates how the left ventricle is filled from two sources in patients with chronic aortic regurgitation.

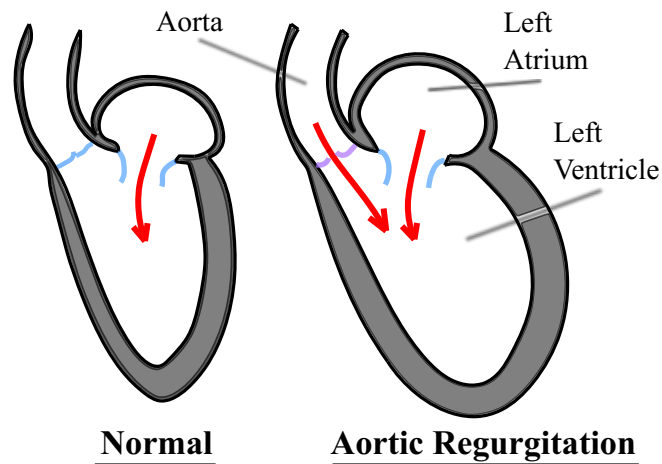


Figure 1.3: Adaptation of chronic aortic regurgitation. Modified from image found in the book entitled “Cardiovascular Physiology Concepts” [14]

Chronic aortic regurgitation occurs when the left ventricle increases in size to compensate for the excess inflow from both the mitral and aortic valve [14]. The increased volume is expected to circulate at the same speed as under normal conditions which leads to hypertrophy of the left ventricle. Hypertrophy results from the extra work that the muscles of the heart endure due to the additional volume ejection performed at the same speed. The extra work performed by the myocardial tissue results in the gain of muscle

mass which tends to prohibit efficient functionality of the heart [15]. Acute aortic regurgitation differs from the fact that the left ventricle does not compensate in a volume change which in turn results in an increased diastolic pressure and decreased systolic pressure due to increased backward flow [16].

1.2.1. Cardiovascular Research

Latest advancements in technology need to be continually integrated into cardiovascular fields of research to further benefit progress. The importance of reliable cardiovascular medical training and device testing is growing proportionally to this trending epidemic. The most common tool used for most testing and training is heart simulators which provide a neutral testing environment. The anatomical correctness of simulators is constantly evolving with an abundance of options becoming available. 3D bio-printing options can now allow the opportunity of producing engineered tissue with increasing complexity which can be applied towards the creation of vascularized constructs, myocardium and heart valve conduits with a precision range of 50-300 μm [17].

1.2.2. Cardiovascular Device Testing

There is extensive research performed on studying the flow across prosthetic heart valves during operation where the ultimate goal is to minimize blood cell damage, coagulation potential and optimize vortex formation. Coagulation is a common build up on prosthetic

heart valve leaflets that form over time and limit the functionality of the mechanical heart valve [1]. Studying these effects can represent a challenge due to the complex geometry of cardiovascular anatomies and flow patterns involved in the cardiovascular circulatory system. The choice of a replacement valve is usually specific to a patient after considering the levels of risk involved, estimated lifespan of the procedure and compatibility of the patient towards anticoagulant medication. Mechanical heart valves made of metal components and bio-prosthetic tissue valves made from either explanted porcine valves or pericardium material [18] are the most commonly offered to patients each with their advantages and disadvantages [19]. Mechanical valves tend to have better resistance to clots, however require a lifelong anticoagulation therapy. Tissue valves behave more like natural heart valves and respect the proper vortex formations formed. However, tissue valves have a shorter lifespan than their mechanical counterparts and therefore are rarely used for children [1] [19].

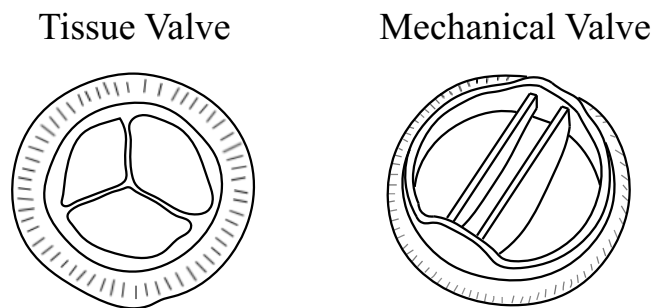


Figure 1.4: Adaptation of both a tissue heart valve and mechanical heart valve.

Modified from image found on “the Drs Wolfson” website [20]

Invasive surgeries along with non-invasive surgeries represent a risk to the patient. Since there are many risks involved with heart valve surgeries many efforts are done towards properly matching patients and procedures in order to avoid multiple surgeries performed

during a patient's lifespan. One good example that demonstrates the importance of pre-installation testing is the history of mechanical heart valves. The Bjork-Shirley mechanical heart valve was approved for public implantation in the early 80's and quickly needed to be recalled due to outlet strut fractures. These failures would send the strut of the mechanical heart valve into the circulatory system leading to fatal consequences. This resulted in a mortality rate of 75% of patients involved and the Bjork-Shirley valves removed from the market in 1986 [1].

In the U.S.A., the F.D.A. (Food & Drug Administration) regulates the approval of medical devices for use by the general public. For prosthetic heart valves, insurmountable proof is required that each device is safe. This is accomplished through extensive clinical trials along with a record of every valve treatment performed in America which is logged into a registry [21]. The need for viable ways to speed up the process when approving new devices is a priority mainly for the reason that people's lives are on the line and time is an important factor. At present, preliminary steps before clinical trials is performed using bench testing and animal testing which leaves a gap in between that could be filled with an adequate intermediary step within the medical device testing process [21]. When testing an implanted prosthetic valve, one of the most important performance measurements is pressure gradients which helps determine the success of the operation [22]. With regards to medical device testing there is still much room for improvements. Interactions of heart valves with patient specific anatomies can now be analyzed with heart simulators before the heart valves are introduced into patients. This will lead to medical devices being designed for patient specific compatibility along with a tested delivery method.

1.2.3. Cardiovascular Medical Training

Although medical training is only touched briefly in this dissertation leaving more emphasis on medical device testing, medical training is still an important option to have on a heart simulator that can perform multiple tasks. The current method for medical training is known as the apprenticeship model which was first introduced in the early 1900's. This method relies on residents shadowing doctors in practice for extended periods of time to learn and perform procedures through imitation and repetition under an expert physician's surveillance [23]. Medical procedures vary greatly throughout the world and the use of the apprenticeship model creates a platform where non-uniformity in medical training becomes very present. After extensive observations of this phenomenon the need for standardization was determined to be important. To answer this need simulation based education has grown in popularity because it can provide an intermediary step between theory and practicing on a patient. This approach is optimizing the educational procedure through improvements of technology with the potential of uniformity in trainings [23]. Simulators provide the opportunity to perform procedures in a repetitive fashion eliminating stress associated with first time interactions with real life patients. Medical simulators of today also create the availability to study pathologies that until now have been difficult or impossible to study. Cardiac surgery professors recognize that simulation training has increased the confidence and technical expertise of their training physicians [24]. The success of simulation-based education is due to the hands on experiences provided by these advancements in technology that improve learning. Easily obtainable medical simulators along with consistent training

methods would increase the ability to implement a standardized medical training curriculum. One example of quantifiable proof that improvements are brought through simulation based medical training is a study that introduced 3D printed heart models into their simulation. Improvements of pediatric resident training results due to the addition of simulation-based trainings showed an increase of 51.7% in knowledge acquisition, 61.4% in knowledge reporting and 73.1% in structural conceptualization and all of this done in a critical care situation [25].

The MaxTron system is capable of patient specific medical training which is destined to increase patient safety. Simulators like these could help assess if a device and introduction method are valid for a specific patient [26]. These heart simulators could also serve the purpose of educating patients and their family members about operational procedures that can sometimes require parental or guardian consent.

1.2.4. Cardiovascular Fluid Dynamics

Cardiovascular fluid dynamic analysis can lead to the creation of mathematical models that help to quantify cardiovascular conditions. Advancements in 3D imaging techniques now permit the creation of patient specific computer generated models. The process makes use of a combination of M.R.I. readings, computed tomography and ultrasound contributions towards deriving equations that describe hemodynamic behaviour [27]. These patient specific models can be used to determine important flow parameters. Vortex formation time and viscous energy dissipation are examples of important areas of

interest when investigating cardiovascular fluid dynamics. These studies advance clinical diagnostic efficiency due to earlier and better evaluations of pathology severity [28]. Present vortex formation studies are limited to 2D analysis. Energy dissipation and other phenomena can be better analyzed with 4D flow data provided by a heart simulator that is M.R.I. compatible [29].

1.3.1. Thesis Objective

Towards quantifying hemodynamic behaviour during cardiovascular circulation in 3D, an innovative approach was taken to develop an M.R.I.-compatible heart simulator named the MaxTron system. Primarily, the M.R.I. compatibility of the fully-coupled (aortic and mitral valves) F.S.I. fluid-structure interaction system will be investigated along with steps and measures that were taken in order to optimize noise reduction during M.R.I. acquisitions. Iterations needed to adapt the heart simulator and activation system to the M.R.I. testing platform will be discussed in the appendix section along with the many configurations of different 3D printed heart components, heart valves and assembly methods used towards optimization of the experiment process. Benefiting from the M.R.I. compatibility of the system, severity progression of aortic regurgitation was monitored in a 3D perspective with respect to time. Intersection vortex formation between different severities of aorta regurgitation and varied mitral valve orientation combinations were visualized using Ensight software (Siemens; Munich, Germany). Both improvements on the availability and user-friendliness of the simulator are directly aimed at impacting patient safety in a positive way. User-friendly guidelines can be

followed to manufacture, assemble and operate this heart simulator at a low cost. With every practicing physician having the availability to procure their own anatomically correct heart simulator, patient safety can be optimized to its fullest potential. Availability of heart simulators also benefits the field of medical device testing by facilitating the certification process which helps deliver these devices to the general public at a quicker rate. Through the process of this present research the following important questions were answered.

- 1) Can a heart simulator and its components be made compatible for M.R.I. experimentation using mostly 3D printed materials and 3D printing manufacturing processes?
- 2) Can these heart components assemble together in an interchangeable system capable of representing multiple severities of a specific pathology?
- 3) Can the replacement of a mitral valve be orientated in such a way as to diminish the side effects of aortic regurgitation?

Chapter 2

2 Literature Review

2.1.1. Cardiovascular *In vivo* Studies

The birth of cardiovascular research dates back to the renaissance. Leonardo da Vinci made observations of the tricuspid valve and sinuses of Valsalva that were both a scientific and artistic homage of admiration to the beautiful clockworks of life [30]. This chapter of this dissertation shall focus mostly on cardiovascular research development throughout history while paying special attention to experimentation regarding observations of left ventricular flow and aortic regurgitation. Early studies dating back to the 1970's were mainly performed on animals like dogs and sheep using cine-angiography which resembles motion picture x-rays. The observations of pressure readings and velocity profiles led to the discovery of stable flow in the left ventricle which was previously believed to be turbulent [31]. Further studies revealed that there is great importance in the ring like vortex formation developed from the mitral valve leaflet tips. This vortex formation permits proper mixing of the circulating blood, evenly distributes pressure along ventricle walls and optimizes flow circulation [31]. All of these early studies would slowly evolve proportionally with the contributions that advancements in technology would start to offer. When echocardiography was introduced in the early 1980's blood circulation could be better analysed and specific characteristics could be determined in a non-invasive manner. The 2D Doppler ultrasound method provided means towards obtaining direction, velocity and turbulence

from observed blood flow. This method proved efficient especially for the study of aortic regurgitation because visualization of the regurgitant jet was made possible in real time [32]. Using 2-dimensional Doppler flow imaging in a similar study that was aimed at grading the severity of mitral regurgitation, researchers noticed different orientations and dynamics of the regurgitant jet which had not been noticed before the use of this method. The correlation between Doppler imaging and angiography were validated with regards to evaluating the severity of mitral regurgitation [33]. Distinguishable flow patterns of specific pathologies were now quantifiable and would lead to better diagnostics. Ultrasound-based techniques offer great potential for capturing measurements by means that have fewer constraints than M.R.I. methods which are restricted by non-ferromagnetic materials, expensive costs and longer post processing times [34]. Despite these facts, M.R.I. readings have proven to be superior than other methods with regards to acquisitions of velocity profiles and flow trajectories in 3-dimensions with respect to time [35] [36]. A method called particle tracing that is used to visualize flow in fluid dynamics was applied to assist researchers using M.R.I. velocity mapping due to their readings being scattered with noise [37]. Another innovative technique using echo sequencing proved to be an effective way to obtain better readings related to flow velocity. This discovery would solve many issues which were related to loss of signal resulting from rapid blood flow [38]. The method is combined with phase contrast cardiovascular magnetic resonance imaging and measurements obtained with this method of blood flow velocities, vector fields, pathlines, streamlines and volumetric quantifications helped the understanding of pathological blood flow dynamics [39]. Another great contribution for cardiovascular research was in 1994 when visualisation of

blood flow using M.R.I. velocity mapping techniques in patients alongside a flow phantom validated further *in vitro* studies using this approach. The study was however limited to a single 2D plane of analysis [40]. These early *in vivo* experiments had many limitations which mostly involved using living patients. Humans are not meant to spend long hours in an M.R.I. scanner like those needed for cardiovascular research and the availability of willing patients with increasing severities of a similar pathology is scarce. The obvious advantage of *in vitro* experimentation is the fact that the process does not involve actual patients and can be performed repetitively with fewer limitations. Further advancements involved using Navier-Stokes equations for incompressible flow to represent pressure fields which were later validated through *in vivo* M.R.I. acquisitions and *in vitro* phantoms. This method provided the potential of discovering relationships between pressure and blood flow within normal and pathology affected cardiovascular systems [36].

2.1.2. Cardiovascular *In vitro* Studies

With the aim of patient safety and bettering research capabilities, *in vitro* experimentation started gaining much deserved popularity. Early studies that were performed using mock setups instead of actual patients were aimed at better understanding heart valve functionality and potential risks involved. There are mainly three types of systems used for the testing of prosthetic heart valves in cardiovascular *in vitro* research which are pulsatile flow (pulse duplicator) systems, steady flow systems or accelerated flow systems which are used for testing the life span of a medical device [41]. Studying the

way a heart valve closes was first performed using a piece of see-through tubing and produced wonderful insight to the fluid dynamics involved [42]. Model left ventricles were constructed in 1972 using a transparent rubber bag submerged in a tank of water. The bag would have both a model mitral valve and aortic valve constructed from nylon netting and silicone rubber in order to direct flow. Circulation of the modeled left ventricle was generated by a piston pump applying and relieving pressure to the filled tank [43], which is an approach still commonly used today. The following figure demonstrates the setup used for that experiment.

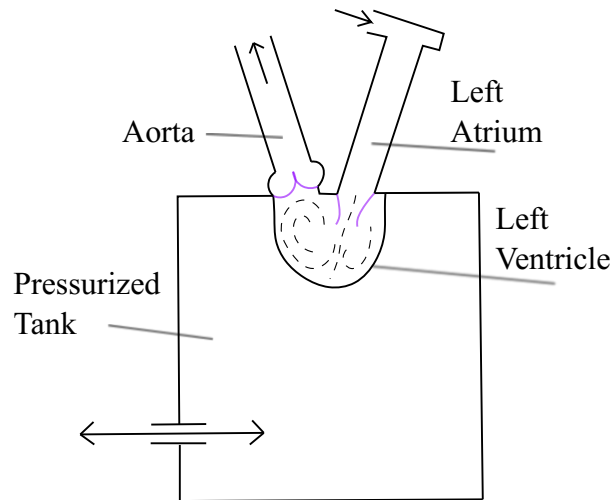


Figure 2.1: Adaptation of the Bellhouse experiment model of left ventricular flow.

**Modified from image found in an article from the “Cardiovascular Research”
journal [43]**

Other studies would focus on closer observations of valve functionality. Innovative prosthetic heart valves were studied to prove their superiority over previous models. Ball valves or disc elements were commonly used as prosthetic heart valves but represented elevated risks of thrombogenic potential. Mitral valves that were designed to mimic

anatomical mitral valve functions were proven to develop the vortex formation required for optimal cardiovascular circulation [44]. Numerous prosthetic valves were analysed with regards to regurgitation using a pulse duplicator. Regurgitation is a common occurrence when dealing with any replacement heart valve that at the present do not close completely as naturally intended. Regurgitation was found to increase proportionally with regards to heart rate and as a result cardiac output was inversely affected [45]. Another study compared the St. Jude bileaflet mechanical valve, Bjork-Shiley tilting disc and Carpentier-Edwards porcine valves. It was found that despite the St. Jude valve having the most regurgitation amongst the valves, it demonstrated the best fluid dynamic performance [46]. Comparison of older and newer designs of commonly used prosthetic heart valves would show differences in peak velocities obtained by each valve during functionality and the results showed that peak jet velocities and turbulence levels were improved by the newer designs. These *in vitro* studies were intended to assist in the selection for patient/valve compatibility and improvements made towards prosthetic valve designs [47].

Color Doppler imaging was optimized through *in vitro* experiments. The use of a left heart pulse duplicator was chosen for a study for the controllability of the system and the possibility of observing regurgitant jets coming from the aortic passage. Laser Doppler velocimetry imaging provides two dimensional readings as opposed to the one dimension obtained from pulsed Doppler flow mapping. This non-invasive method of determining severities of aortic regurgitation was preferable over contrast angiography that requires invasive catheterization. Aortic regurgitation was graded in that experiment by maximum length and width of the jet along with color variance due to turbulence [48].

2.1.3. Cardiovascular Research of Today

Recent contributions of computer simulations have been helping develop sophisticated tools useful for cardiovascular research. Extensive 3-dimensional studies of mitral valve orientation were done using a computational approach. The computed inflow showed variations depending on the orientation which was validated visually with the *in vitro* setup but quantitative validation required 3-dimensional *in vitro* data not available during the time of the study [49]. Thromboembolism is still a major disadvantage of prosthetic heart valves and studies are continuously being done to provide improvements. Cardiovascular simulators and 2D software simulations play an important role in this field of research. The main objective of these studies is to minimize stagnation zones and regions of elevated stress associated with these medical devices to a level that eliminates the need for anticoagulation medicine commonly prescribed with heart valve replacements [50].

The evolution of M.R.I. acquisitions has also continued to prosper. M.R.I. data was first obtained using 1.5T (Tesla) machines but slowly transitioned to 3T machines due to improved data readings. First the head and then the body were scanned with 3T M.R.I. Scanner but cardiovascular magnetic resonance was slower towards the transition. The continuous fluctuations of the heart and the closeness of the heart to the lungs led to low signal to noise acquisitions. The increase in magnetic magnitude was eventually beneficial and increased the signal to noise ratio which allowed easier readings of the results [51]. Numerical methods along with *in vivo* M.R.I. data were used in combination in order to predict patient specific intra-ventricular flow. ANSYS Fluent (ANSYS;

Canonsburg, PA, U.S.A.) software was used to simulate 2D intra-ventricular flow which was validated with *in vitro* and M.R.I. *in vivo* data. The asymmetric shape of the mitral valve was shown to direct the mitral inflow jet towards the posterior wall [52].

Recent studies that were performed *in vivo* with open-chest dogs were focused on observing energy loss from aortic regurgitation. They came to the conclusion that using vector flow mapping was an efficient method to determine the severity of aortic regurgitation because diastolic energy loss would noticeably increase proportionally to the disease severity [53]. L.C.F.D. colleague Dr. Giuseppe Di Labbio studied progressive chronic aortic regurgitation by recreating different severities of the heart disease with the use of an *in vitro* system created by him and fellow Capstone team members. The data obtained revealed a reversal of the vortex created in the left ventricle due to severe aortic regurgitation along with an increase in viscous energy dissipation [28]. Continuation of Di Labbio's studies showed that all severities of aortic regurgitation seem to create turbulence within the left ventricle and also affect the central vortex formation which is supposed to optimize circulation and blood mixture. The results of these studies were obtained using P.I.V. measurements in 2-dimensions [28]. These results coincide with another study obtaining similar results, namely that the incoming regurgitant jet prohibited the mitral inflow from creating proper vortex formations and increased energy dissipation within the ventricle proportional to the severity of aortic regurgitation [12].

2.2.1. Cardiovascular Simulators

There are four main categories of simulators at the moment that are used for medical training, medical device testing, and cardiovascular fluid dynamic analysis. Firstly, computer-based learning is a method that makes use of computers for educational training and simulations. Secondly, phantoms are devices that model specific anatomies of interest and can be customized for training of specific skills or research. Thirdly, computer-assisted mannequins which are full body simulators with a computer interface and combined offer the ability to simulate specific scenarios like critical care situations. One of the most recent additions is virtual-reality simulators which create an immersive experience which can be combined with haptic feedback [23]. This list shall continue to grow as advancements in technology persist. A commonly used heart simulator throughout the world that performs similar experiments as this presentation is the ViVitro's pulse duplicator (Starfish Medical; Victoria, Canada). Their pulse duplicator has gained popularity for its well-known capability of reproducing several cardiac pathologies. The system has setting controls that can alter the peripheral resistance, as well as the compliance of the system which can help study different extents of a certain disease. Pressure readings can be obtained from both the aortic and mitral valves. The flow is powered by a pump in a pulsatile fashion which is adjustable in order to mimic certain conditions of flow interactions with the prosthetic valves. Blood circulation can be measured with their ViVitro data acquisition system and can be used to analyze the performance of each cardiac device [54]. A more recent development by ViVitro laboratories entitled the ViVitro Endovascular simulator can simulate any possible

section of the cardiovascular system due to its user-friendly reconfigurations. This model is very useful for training a multitude of transcatheter or surgical vascular interventions as well as medical device testing [55].

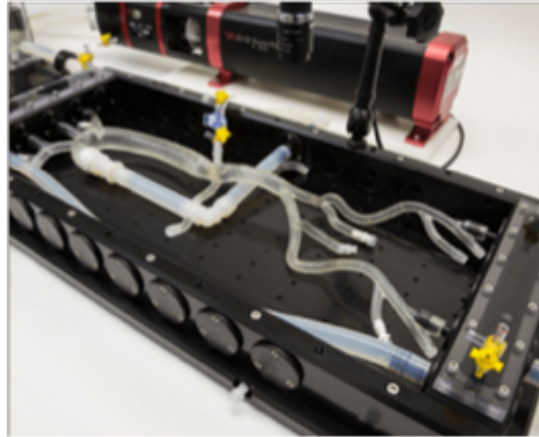


Figure 2.2: ViVitro Labs Endovascular Simulator [55]

The above figure demonstrates the bulkiness of the Vivitro Endovascular simulator that contains metal components which prohibit the system from being used in an M.R.I. scanner. The system also does not include heart cavities and fails to represent patient specific anatomically correct heart components.

2.2.2. 3D Printing-based Heart Simulator

The L.C.F.D. laboratory is supervised by Dr. Lyes Kadem who has led many consecutive undergraduate teams and graduate students through cardiovascular fluid dynamic research innovations and continues to breach the forefront of this field's advancements. The heart simulator built for this dissertation aims to answer the growing need for

anatomically correct heart simulators that can represent any pathology when simulating patient specific anatomies for medical device testing along with non-invasive delivery methods. MaxTron builds off the ideas used in previous iterations built in the L.C.F.D. laboratories with the objective of advancing M.R.I. compatibility, increased portability, interchangeability, user-friendliness, availability and aesthetic appeal of the system all while reducing costs and need of technical skills to operate. This is achievable by finding methods of manufacturing that reduce the cost and if possible create a heart simulator that can be used for multiple tasks/experiments which reduces the need to buy multiple types of systems. One of the main approaches for most of the objectives was to take advantage of the advancements in 3D printing which helped with user-friendliness, availability and reduction of cost. An added advantage is the increase in lifespan of the 3D printed heart components when compared to their silicone counterparts. An example is the artificial heart made by Functional Materials Laboratory at the Swiss Federal Institution of Technology in Zurich, which was made using a lost-wax casting method to make a 3D printed silicone heart named the Soft Total Artificial Heart (sTAH). The inconvenience of their remarkable innovation is the lifespan of the heart which is measured to be an average of 3000 beats which represents about 30 to 40 minutes of functional running time [56]. L.C.F.D. 3D printed heart components were printed with 0.1 mm layers within a potential layer resolution range of 0.05 - 0.4 mm. 3D printed heart components created for this project demonstrated endless usability and lasted the entirety of the project duration. M.R.I. compatibility for an *in vitro* setup offers a chance to achieve 3D acquisitions of pathological hemodynamic interactions that have until now been unavailable.

Chapter 3

3 Methodology

3.1.1. State of the Art

Cardiovascular research has evolved gradually with the help of advancements in technology. Many restrictions and design iterations were required to make a cardiovascular simulation system that could be introduced into an M.R.I. scanner. These efforts are done to advance cardiovascular fluid dynamic research with the hope of finding numerous solutions towards prevention, diagnostics and patient care. Well-designed experiment setup's that can be performed at a rapid pace are truly beneficial for M.R.I. experimentation which can be cost heavy. The following will explain the methodology behind creating an *in vitro* model capable of representing the complete anatomical heart and functional cardiovascular system along with preparations, procedures and acquisition details when using the system in an M.R.I. scanner.

3.1.2. The MaxTron System

In order to achieve representation of the complete heart, the system is devised into two separate systems to have complete control over pressure levels in each subsystem of the model heart. The current design needed the reservoir of water for the left side of the system to be placed at a higher altitude than the right side reservoir in order to mimic physiological conditions. Many left ventricle *in vitro* experiments rely on the pressure

changes of a tank of fluid to activate ventricle compressions much like the apparatus used in early works of Bellhouse [43] up to more recent studies performed by Di Labbio [28]. The MaxTron model makes use of a hydraulic system that activates ventricle compression by physically squeezing the ventricle between a pusher and a customizable support structure. Pressures in a healthy left ventricle and aorta can attain amplitudes of 120 mmHg [6] and the right ventricle can attain peak pressures closer to 25 mmHg [57].

Figure 3.1 illustrates the overall setup which mainly consists of reservoirs linked to 3D printed heart components housed inside a fiberglass mannequin torso and activated by a hydraulic system involving many components. Similarly, both separate circulatory systems begin by their respective reservoirs emptying into 40 Shore A hardness tubes which lead to valves that help control pressure, flow rate and mimic capillary resistance. Fluid in these experiments was regular water and not a water-glycerol solution due to the numerous iterations taking place during the entirety of the project which would have required extensive cleaning. Upon activation of the left ventricle, the wall is compressed pushing fluid through the aortic valve and this segment of the cardiac cycle is known as the systolic cycle. The fluid then makes its way down the aorta through the base of the mannequin and the flow is eventually recycled back into the reservoir completing the left loop of the cardiovascular circulatory system. When the left ventricle is decompressed, this reduces the pressure in the chamber allowing the aortic valve to close and for the mitral valve to open refilling the left ventricle known as the diastolic cycle. The right side functions the same way as the left side of the system, but at a lower pressure of approximately 95 mmHg difference.

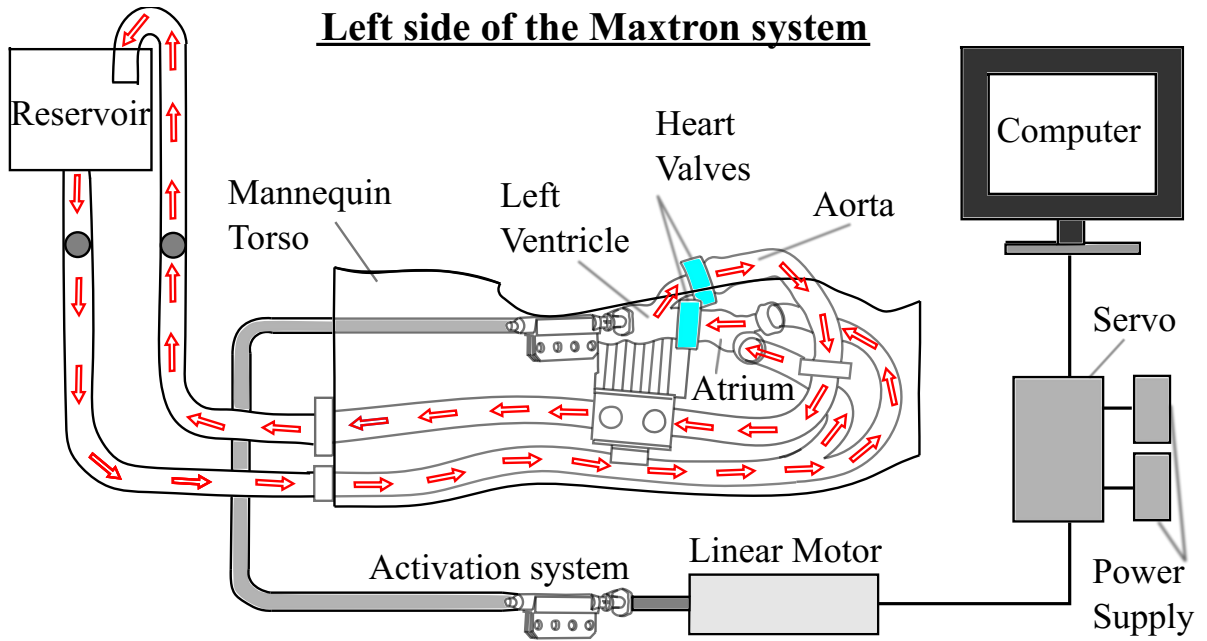


Figure 3.1: Schematic overview of the left side of the Maxtron system

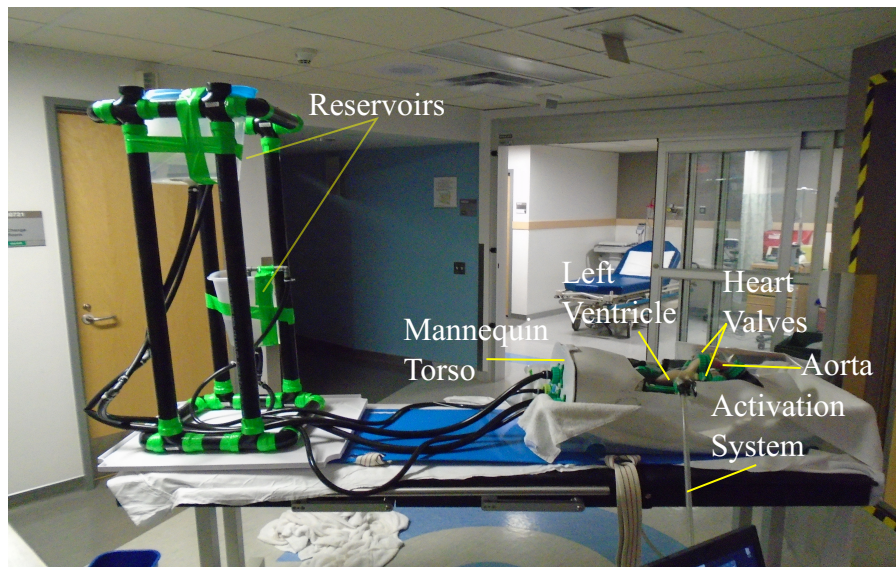


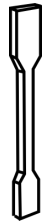
Figure 3.2: The Maxtron System

Figures used in this dissertation were mostly created with the help of Inkscape (Free Software Foundation; Boston, MA, U.S.A.)

3.1.2. Simulator Casing Considerations

Many parameters needed to be considered for the casing of the heart components and other functional items which are essentially the bulk of the system. Since the apparatus is intended for M.R.I. compatibility the system needed to be mobile and compact. The use of a male mannequin torso was chosen to house the system because it had the right dimensions, added to the realism of the simulation and could retain any water leakage that could occur during operation. Any water leakage even minimal could have devastating consequences on the expensive M.R.I. equipment. The inside of the mannequin torso was lined with a custom designed rail track system that enables interchangeability of the support structures that hold the heart components, hydraulic activation systems, and multiple tubing connections. The choice of material for the rail track system was P.L.A. 3D printing filament. P.L.A. filament has very close properties compared to A.B.S. filament but was chosen mainly to respect laboratory regulations with respect to emissions given off during 3D printing. The 3D printer used was a Lulzbot Taz 6 (Aleph Objects; Loveland, CO, U.S.A.) capable of printing both solid and flexible 3D prints. The following P.L.A. mechanical properties from the Ultimaker (Ultimaker; Utrecht, Netherlands) P.L.A. filament used were obtained using the ISO 527 testing method at a testing speed of 50 (mm/min) [58].

Table 1: Ultimaker P.L.A. 3D Filament Mechanical Properties [58]

	 3D Printed Sample
Infill	100%
Tensile strength at yield (MPa)	49.5
Tensile stress at break (MPa)	45.6
Hardness (Shore D)	83
Elongation at break (%)	5.2%
Tensile modulus (MPa)	2346.5

The cross section of the rail track system was designed to withstand the forces present during operation which include shear, torsional and tensile considerations all while considering weight restraints.

3.1.3. Heart Components

In total the system consists of six heart components, three for the left side of the heart and three for the right side of the heart. The left side heart components are commonly known as the left atrium, left ventricle and the aorta and the fluid circulation passes through the components in that order in a one-directional circulation. The right side heart components are commonly known as the right atrium, right ventricle and the pulmonary artery and the one-directional circulation passes through the components in that order. Usually heart components in the L.C.F.D. are made from applying layers of silicone upon a 3D printed model of the desired heart component. 3D Models of the heart components originated from C.T. and M.R.I. scans (Solid Heart Gen 2, Zygote; American Fork, UT, U.S.A.). After many coats the flexible silicone can be removed from the model and be used for *in vitro* experimentation. These silicone heart components have the advantage of being created with complete control over flexible compliance and transparency. Silicone heart components were successfully implemented into the system but focus of this dissertation was maintained around the more durable, user friendly methods and accessibility of 3D printed heart components. Tests were done to see the best way to print the heart components using NinjaTek 3D printing flexible filament named Ninjaflex (Fenner Inc; Manheim, PA, U.S.A.) which has the following properties [59].

Table 2: Ninjaflex Filament Mechanical Properties [59]

	 <p>3D Printed Sample</p>
Infill	100%
Tensile strength at yield (MPa)	4
Tensile stress at break (MPa)	26
Hardness (Shore D)	85
Elongation at break (%)	660%
Tensile modulus (MPa)	12

The heart components were printed as thin as possible for elasticity purposes with wall thicknesses of 1 to 1.2 mm. The 3D modeling of the heart components were performed on Solidworks (Dassault systemes; Velizy-Villacoublay, France) which is a three dimensional modeling software. Once a 3D model is made on Solidworks, the file can be saved as an S.T.L. file and introduced into the CURA (Ultimaker; Utrecht, Netherlands) slicing program compatible with the 3D printer being used. Within the slicer interface many parameters can be chosen to optimize the success and material properties of the component. The left atrium that has four small connections and one large connection represents the most complex heart component to 3D print. One optimal way to successfully print the left atrium component is to position it at an elevated angle which

minimizes the gravity induced complications of the print. Once completed and assembled, tests proved that thicker components could retain impermeability however thinner components of 1 mm or 1.2 mm thickness were not impermeable and droplets of water from the circulation would bleed through the material. A solution brought forth by Dr. Lyes Kadem of using a secondary product to line the heart components with a water-proofing membrane was implemented. The only restriction was that the medium needed to be easily accessible to the general public. Many water-proofing products and techniques were tried but the most efficient and easily accessible product that required minimal skill to apply was a temporary roof repairing product named Leakseal (Rust-Oleum; Vernon Hills, IL, U.S.A.). After applying an average of 5 coats on the outside of each component, the components were able to retain the pressures needed without any leakage and later proved to be robust enough to endure the friction and pushing motions applied by the hydraulic activation system for the entirety of the experimentation. Another benefit from using Leakseal was the fact that pieces could be easily sprayed after getting cut up and sewn back together which facilitated the many iterations performed. The maximal pressure limit attainable by the sprayed 3D printed heart components was not tested but was found to be more than adequate enough for the pressures they were subjected to during operations. Luer tapered connectors were placed on the four areas of interest that would provide access to obtaining pressure readings from the aorta, left ventricle, pulmonary artery and right ventricle.

Echocardiography readings were attempted on the system but regrettably the filament used for the 3D printed heart component was not compatible. This avenue was not further explored due to time limitations.

3.1.4. Screwclamps

In order to connect the heart components to each other and the tubing that would complete the circulation, customized clamping devices were designed and created which were named Screwclamps because the clamping is achieved by screwing two pieces together. To differentiate the Screwclamp pieces they were simply named female and male Screwclamp components. The Screwclamps were made from 3D printing for M.R.I. compatibility. The first limiting parameter was space therefore the Screwclamps were designed as small as possible all while resisting the forces they were subjected to. The weakest portion of the ensemble was found to be on the female Screwclamp component, namely the thickness of the outer wall was of particular importance. Iterations revealed that the minimal thickness that could be used for the female Screwclamp components was approximately 2 mm which was tested and proved through trial and error. The threading of the Screwclamps was created to endure a clamping force that would secure the pieces together but would fail if tightened too hard in a manner that did not harm the Screwclamp or the heart components. The Screwclamps are also used to secure the heart components to the heart support structure, described below, in a fashion that limits movement and increases predictability of the pressure waveform acquisitions. The heart support structure is conveniently shaped so that the Screwclamps line up in their respective places and can be secured in place with tie-wraps which are easy to remove and inexpensive to replace.

3.1.5. Heart Valves

There are four heart valves used in the system that direct fluid circulation in a single direction. The reason the heart components are separated into six components is to enable access to where the heart valves are located for interchangeability purposes. Between the atrium and ventricles, mechanical, Lifelike (Lifelike Bio Tissue, ON, Canada) and three leaflet bio-prosthetic valves were tested. Between the left ventricle and the aorta on the left side of the heart, different sizes of prosthetic tissue valves were tested which is the same valve used on the right side between the right ventricle and the pulmonary artery. The bio-prosthetic heart valves that were used were the Biocor (Edwards Lifesciences; Irvine, CA, U.S.A.) 25, 27 and 31 mm prosthetic heart valves.

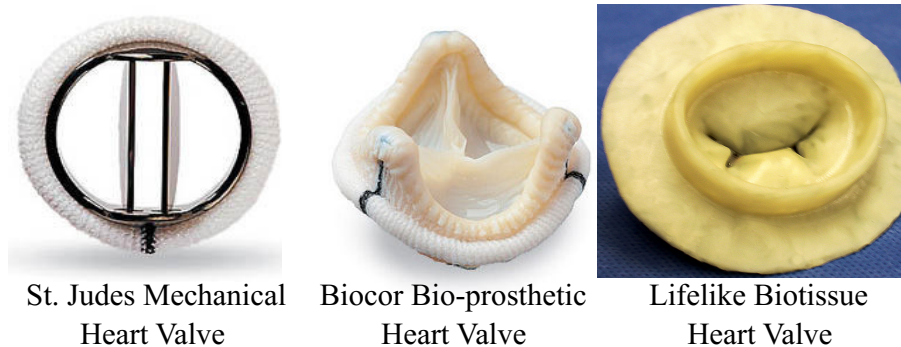


Figure 3.3: Representations of the heart valves used during project iterations.

Images were found at the “Heart Valve Surgery” and “Lifelike Bio-tissue” websites

[60] [61] [62]

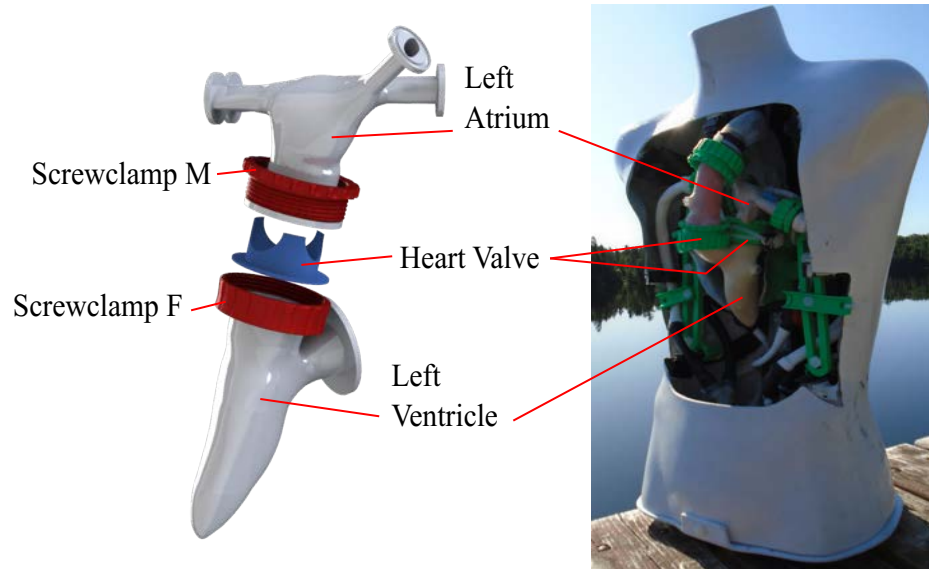


Figure 3.4: Assembly of valve placement between the left ventricle and the left atrium clamped together using a custom made Screwclamp

3.1.6. Heart Support Structure

The current heart support structure was designed and configured for this set-up containing these specific heart components prepared for aortic regurgitation representation. The set-up included patient specific heart components that represent those of a healthy heart but if any changes were brought to either of the components, configuration, hydraulic activation system or pathology represented, the heart support structure could easily be customized with 3D modeling software and 3D printed within an adequate time lapse. The heart support structure is printed using P.L.A. 3D printing filament and is secured into place with attachments that are secured to the rail track system with much care taken towards minimizing unwanted movement.

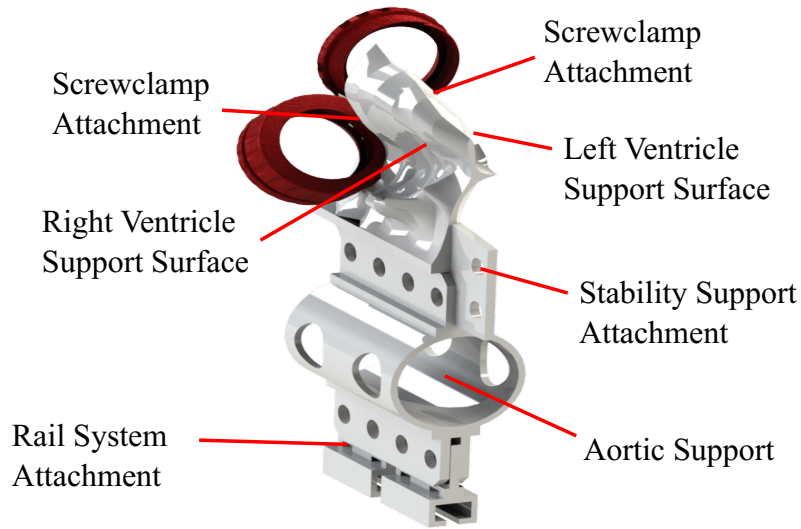


Figure 3.5: Heart Support Structure

3.1.7. Hydraulic Activation System

The hydraulic activation system is mainly driven by an electromagnetic linear motor (LinMot P 01-37 x 120, NTI AG; Spreitenbach, Switzerland) that creates a back and forth motion that can be set to represent different bpm's with an adjustable stroke length. Stroke length used was 60 mm which facilitated experimentation at 70 bpm. According to the specifications, the linear motor can deliver up to 120 N of axial force. The servo drive for the motor (Servo Drive E1100-RS, NTI AG; Spreitenbach, Switzerland) helps regulate bpm and stroke length through the Linmot Talk 6.8.interface. The same interface was used to make an amplitude waveform of 32-bit positional resolution to power the linear motor in a fashion that represented the functionality of a normal heart. The linear motor following the given waveform is attached to the hydraulic pushing system that consists of medical syringes connected to each end of a high pressure flexible

P.V.C. tubing of 70 A shore Hardness with polyester braided reinforcements that is filled with brake fluid as a hydraulic medium. The linear motor pushes the end of one syringe that then transfers force through the brake fluid to the other syringe. The end syringe is attached in a way that the incoming force is transferred to the ventricle it is trying to activate. The end of the hydraulic system attached to the linear motor was mounted with a 30 mL syringe which was 3 times larger than the 10 mL syringe mounted on the pushing end. This helped compensate for the losses obtained along the 11 meter stretch of hydraulic tubing needed for M.R.I. experimentation. The end of the syringe that pushes onto the ventricle is mounted with an interchangeable pusher tip that can be changed in size and shape to help calibrate the pressure readings obtained by the pressure sensors. Although the activation system does not compress the ventricle uniformly from all its sides, this compromise was needed to ensure M.R.I. compatibility within the time frame that was presented. Atrial activation was performed briefly during early experimentation where additional pushers were added and aimed at the atrium during its respective systolic cycle. This iteration was not pursued further due to limited functionality of the linear motor. Pressure results obtained from the presented experiments therefore only account for the E-wave of the cardiovascular cycle. The missing A-wave is commonly found in patients with atrial fibrillation. Atrial fibrillation is a disease where the atrial upper chambers of the heart beat irregularly and is found in approximately 30% to 40% of patients that are also suffering from heart valve complications [63].

3.1.8. Aortic Regurgitation

Although the simulator is capable of representing the complete heart, focus was driven towards the left ventricle specifically to observe simulated progression of aortic regurgitation, amongst the numerous pathologies that could have been represented using this system. In order to recreate different severities of aortic regurgitation, the aorta sinuses were fitted with hemostasis valves and 1 mm diameter transparent fishing wire was introduced. The heart valves were aligned with the aortic sinuses at 120° separation allowing control of the leaflets. The guide wires limited the leaflets ability to close and markings along the wire helped test five to nine severities of aortic regurgitation with assured repeatability. As severities of aortic regurgitation would increase, the closing of the leaflets were increasingly restricted allowing backflow into the ventricle. A photograph of each aortic regurgitation severity was taken with a Rebel Sony camera (Sony Corporation; Minato, Tokyo, Japan) and the R.O.A. (Regurgitant Orifice Area) was computed using the photographs and AutoCAD (Autodesk; San Rafael, CA, U.S.A.) software. After every acquisition, the model had to be removed from the M.R.I. scanner to set the next severity which was designed to be performed in the least amount of time possible. Although the setup was repeatable to a respectable accuracy, there is still room for improvement at representing this pathology in this system.

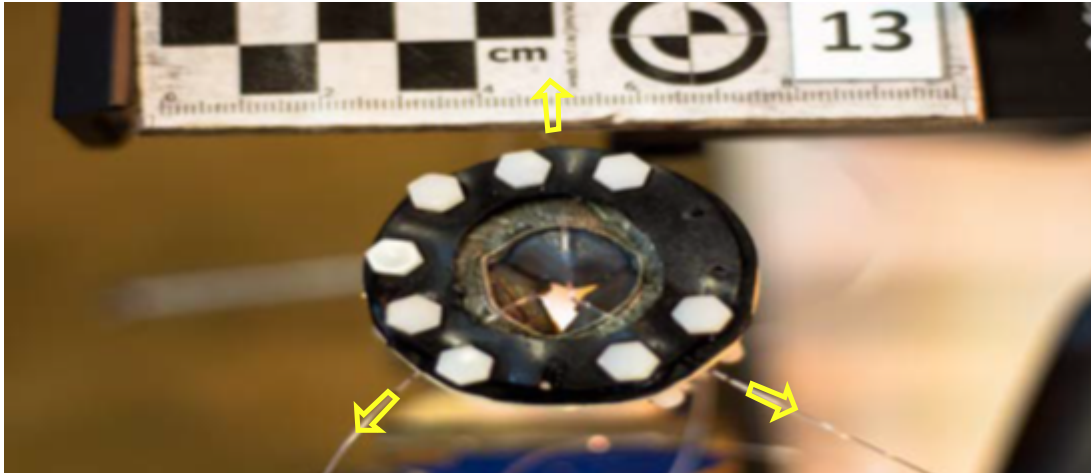


Figure 3.6: Aortic regurgitation setup

3.1.9. Mitral Valve Orientation

In vitro studies about mitral valve orientation effects show important variations when compared to normal flow patterns. Varying prosthetic heart valves, valve geometries, flow rate and heart rate all contributed to the recorded differences. One study proved that there are different valve orientations that optimized ventricular flows for each prosthetic valve tested [64]. Having access to the mitral valve position in the simulator, acquisitions were made at two different orientations by rotating the mitral heart valve. The objective was to determine the effect on flow patterns within the left ventricle during diastole when interactions between progressive severities of aortic regurgitation are combined with a different mitral valve orientation. Trying to achieve the same results *in vivo* would prove to be very difficult, if not impossible and typical data retrieved from similar research is usually in 2D. Having the ability to study these controlled effects in three dimensions has until now been unobtainable.

3.2.1. Magnetic Resonance Imaging

In order to explain the basic principles and functionality of an M.R.I. scanner in as much of a concise way as possible, many facts were omitted and the following represents but an overview of the underlying science. Important factors that make M.R.I. acquisitions possible are the synchronization with the patient's ECG signal and the quickness of the acquisition which is restricted to the time a patient can potentially hold their breath. The main component is the use of magnets which are represented in the following figure. The field generated by the main magnet core represented by B_0 is aligned parallel with the length of the patient and is considered the z-axis of the reference coordinate system [65].

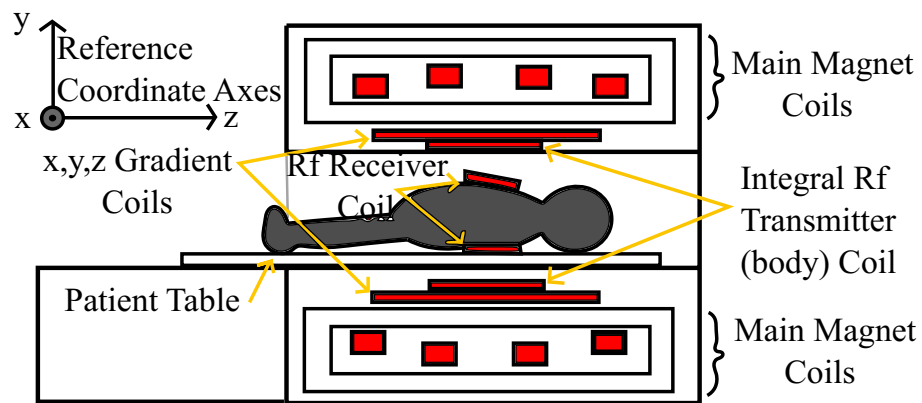


Figure 3.7: Adaptation of the x, y and z gradient coils, integral Rf (Radio frequency) transmitter body coils and the main magnet coils which are used to make M.R.I. acquisitions possible. The reference coordinate system used is also demonstrated.

**Modified from image found in an article of the “Journal of Cardiovascular
Magnetic Resonance” [65].**

The magnetic fields are generated by the main magnet coils, three gradient coils for the x, y and z directions and an integral Rf transmitter coil which each produce a different type of static or pulsatile magnetic field. The strength of the B_0 magnetic field is approximately 60000 times stronger than the earth’s magnetic field when operating at 3T [65].

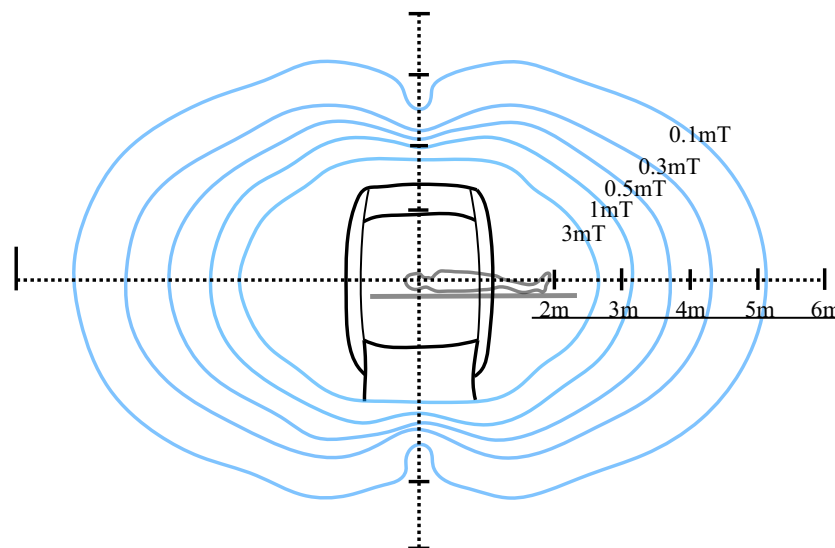


Figure 3.8: Adaptation of the magnetic field surrounding an M.R.I. scanner.

Modified from image found on the “Radiology Key” website [66]

The three gradient coils produce magnetic fields that can be turned on and off very quickly and are aligned in the same z-direction as the B_0 field. Their strength varies along the x, y and z directions and the units used for these fields are milli-teslas per meter (mT/m). The radio frequency magnetic fields produced by the Rf transmitter coils are

generated in an oscillating fashion or a pulse. The frequency is controlled and measured in units of megahertz and the pulsatile field is represented as B_1 in the following figure. The radio frequency applied is found using the Larmor equation from which the resonant frequency or Larmor frequency can be calculated [65].

$$\omega_o = \gamma * B_o$$

γ is the gyromagnetic ratio which is usually 42.6 MHz/Tesla and when using a 3T magnetic field B_o , the resonant Larmor frequency is approximately 127.8 MHz. This resonant frequency is a pulsatile force and the combination of static and pulsating magnetic fields allows signals to be spatially localised and encoded in order to make an M.R.I. image. An addition specifically for cardiovascular M.R.I. imaging is the application of an Rf receiver coil which helps maximise the signal received from the heart [65].

3.2.2. Molecular Nuclei Magnetisation

Essentially, the MR signal is captured from water or fat within the patient's tissue and the process begins at an atomic level. Nuclei with an odd number of protons are known as MR-active nuclei and have the capability to line up easily with magnetic fields. Important elements that have MR-active nuclei include Hydrogen, Carbon, Nitrogen, Oxygen, Fluorine, Phosphorus and Sodium [67]. Nuclei of these elements produce a small magnetic field for each proton and the net magnetic moment has a tendency to align with or against the direction of the B_o field where an equilibrium state is found.

Upon application of the Rf pulse, the net magnetisation of molecules is pulled away from its equilibrium state and rotates around the z-axis at the same frequency as the resonant frequency which is known as precession. The stronger the rf pulse is, the further away from equilibrium the molecules alignment will get and the angle of precession will reach a determined value known as the flip angle. Net magnetisation is represented as M_o and when it is aligned with the z-axis is known as its equilibrium position. The angular rotation produced during an Rf pulse can be divided into two directional components. The angle made with the z-axis which is known as the longitudinal component and is represented as M_z . The other directional component within the x-y plane is known as the transverse component and is represented as M_{xy} .

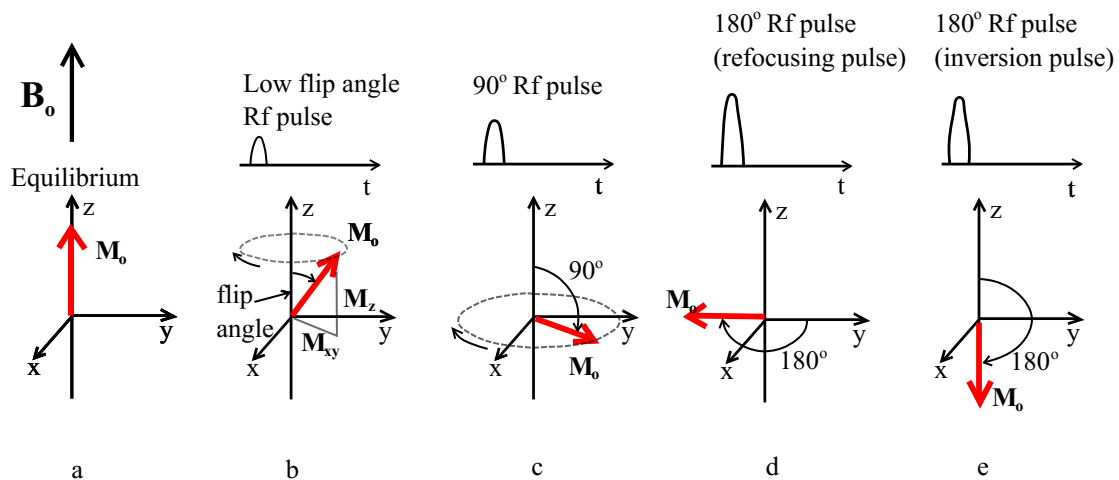


Figure 3.9: Adaptation of the net magnetisation M_o equilibrium which is aligned with the z-axis. During the Rf pulse, the angle between M_o and the z-axis is comprised of both the M_z component, the angle between M_o and the z-axis, and

M_{xy} component which lies in the x-y plane. Modified from image found in an article of the “Journal of Cardiovascular Magnetic Resonance” [65]

This transverse component of the rotation creates its own small magnetic field which can be captured by the Rf receiver coils as an MR signal. In the absence of the Rf pulse, the spin of the molecule rapidly returns to its equilibrium state at a rate known as relaxation time [65]. The longitudinal component of the angle will relax back towards the z-axis at a rate denoted as the T1 time constant and the transverse component will decay its rotation and signal intensity at a rate denoted as the T2 time constant. T1 relaxation time corresponds to the loss of energy as it returns to equilibrium which is dependent on the size of each molecule. Fat molecules are of a size where their rotation or tumbling rate is close to the Larmor frequency which increases the potential for energy exchange and therefore makes fat tissues have fast relaxation rates. Water having a smaller molecular size has a quicker tumbling rate than the Larmor frequency and therefore exchanges energy less efficiently [65].

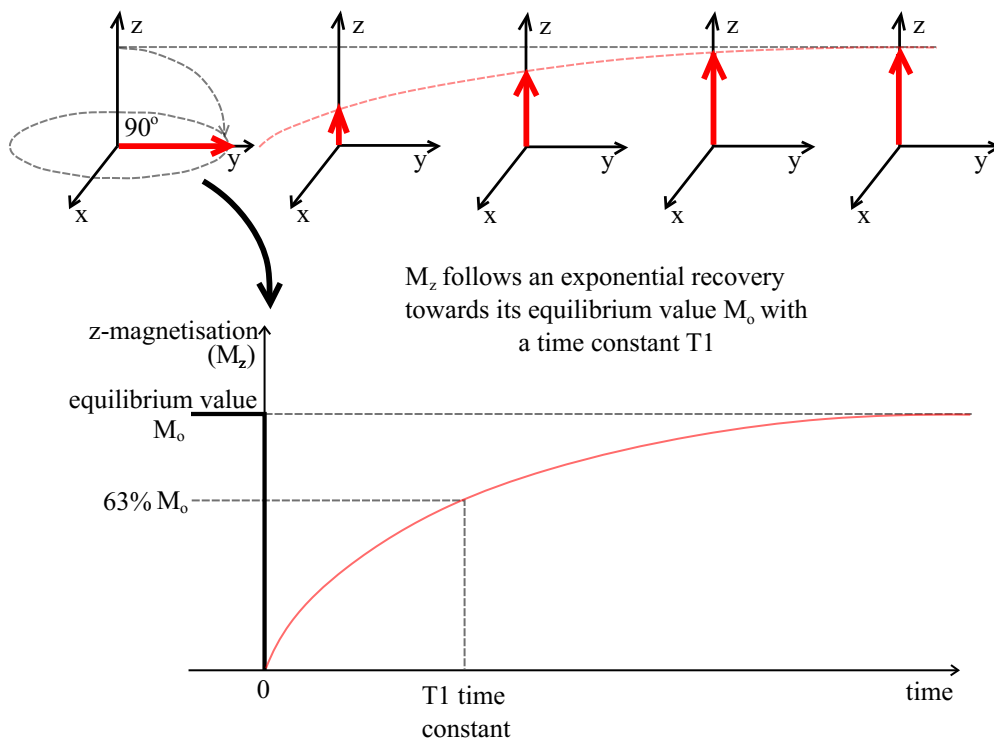


Figure 3.10: Adaptation of T1 relaxation after 90° Rf pulse of the M_z component.

T1 time constant is evaluated at 63% of total relaxation time. Modified from image found in an article of the “Journal of Cardiovascular Magnetic Resonance” [65]

Close proximity to neighbouring proton spins causes T2 relaxation referred to as spin-spin relaxation. This phenomenon can be very random and is therefore irreversible. Spin-spin relaxation along with inconsistencies in the B_0 magnetic field are accounted for in T2* relaxation, determined from the actual rate of decay which is known as the F.I.D. (free induced decay) signal. The T2* time constant is represented in the following figure [65].

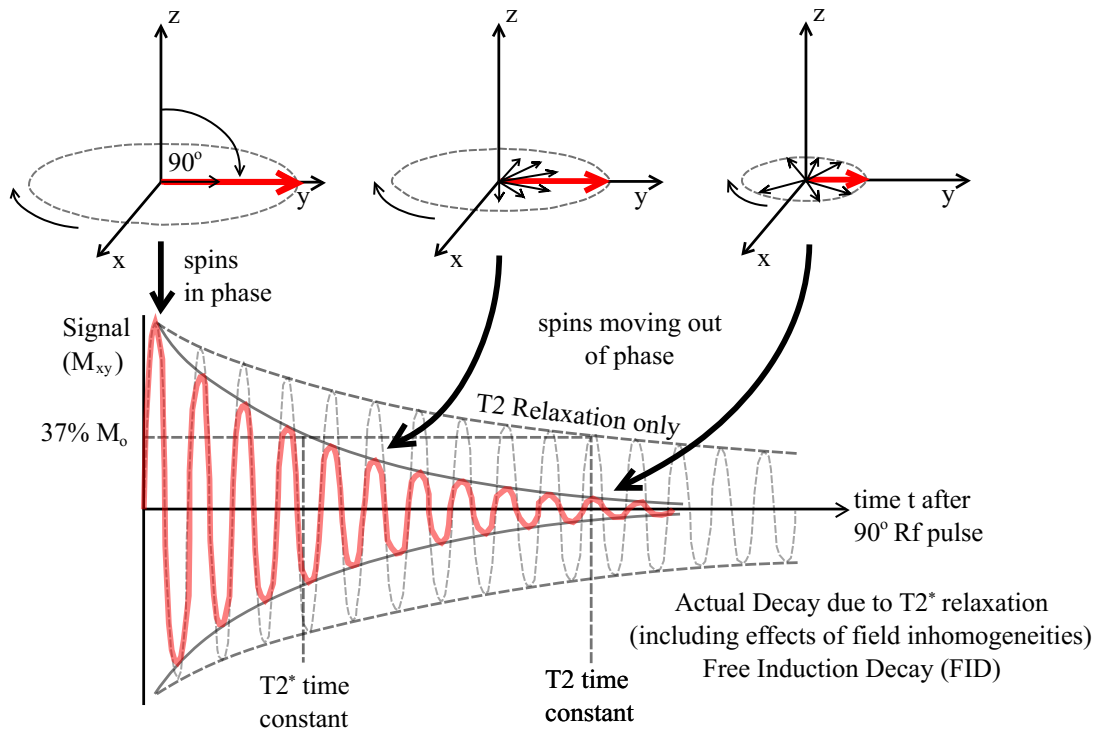


Figure 3.11: Adaptation of the transverse component relaxation after 90° Rf pulse.

T2* relaxation is the term used for loss of phase coherence and T2* time constant represents 37% of initial decaying value after Rf pulse. Modified from image found in an article of the “Journal of Cardiovascular Magnetic Resonance” [65]

An Rf pulse that causes the net magnetisation to move 90° away from the z-axis is known as a saturation pulse which is used to initiate spin echo-based pulse sequences. Low flip angles below 90° as used in the present experiments can be flipped at a quicker rate which is used to make gradient echo pulse sequences. This method is required for faster imaging applications. Following the 90° saturation pulse the z-magnetisation for all tissues returns to equilibrium according to their respective T1 relaxation rates. The

following 180° inversion pulse inverts the z-magnetisation for all tissues which then recover from their negative or positive values as it flips back and forth with continuous 180° inversions. The imaging pulse sequence that is afterward applied creates a contrast which demonstrates shorter T1 relaxation rates like fat tissues that are captured as the highest signal intensities and can therefore be differentiated from other tissue [65].

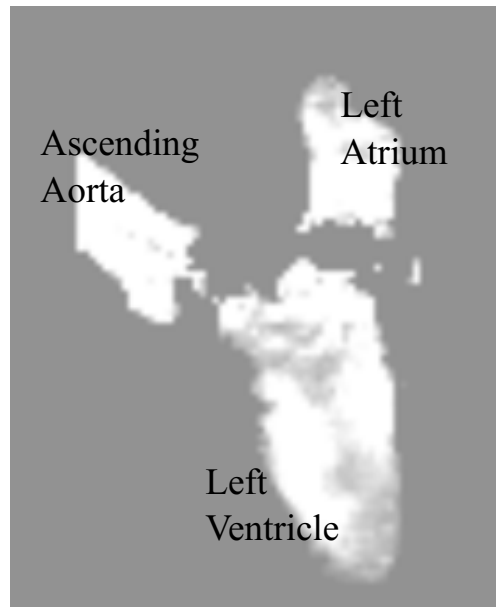


Figure 3.12: Contrast obtained in M.R.I. results of the simulator’s left ventricle

The net magnetisation involves the magnetic moments of all the protons to rotate in a coherent fashion and pointing in the same direction during Rf pulses. The instantaneous angle of the direction is known as the phase angle. When the spins have the same phase, they are said to be in-phase and demonstrate coherence. As previously mentioned, there are two things that can cause a loss in coherence of the spins and therefore loss of signal. Firstly, the interactions that can occur between protons magnetic fields known as spin-spin relaxation and secondly are the potential imperfections within the applied magnetic

field B_0 . F.I.D. can be detected and used to create MR imaging but a more common practise is to measure the MR signal in the form of an echo for which the two main types are gradient or spin echoes [65]. Spin echoes are created by the use of 180° inversions from the Rf pulse. To remove field non-uniformities, the spin de-phasing is completely reversed by the end of the echo time. Spin echo signals are stronger and are less affected by the presence of metal components but acquisition times are much longer therefore gradient echoes are more commonly used. Gradient echoes require additional control over magnetic field gradients. The first positive magnetic field causes proton spin to de-phase whereas the following negative magnetic field gradient reverses the de-phasing resulting in the recovery of the F.I.D. signal [65].

3.2.3. M.R.I. Acquisition Steps

The first step for M.R.I. acquisitions is setting up the slice selection gradient, denoted as G_s , which causes the strength of the magnetic field to depend on location along the z-axis where the Larmor frequency will resonate with patient tissues at a desired plane or slice in the field. The gradient field is activated at the same time as Rf excitation pulse which corresponds to the Larmor frequency at a chosen point along the z-axis. The range of frequencies established by the Rf pulse is known as the transmit bandwidth and determines the thickness of the desired slice [65].

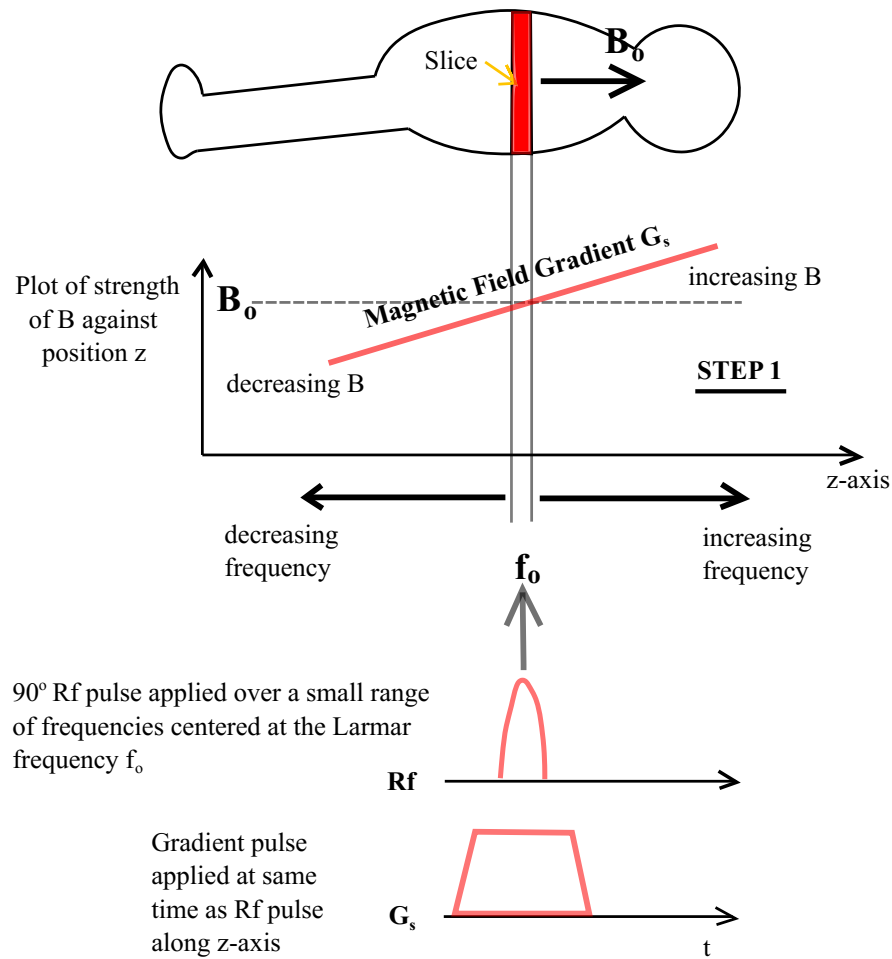


Figure 3.13: Adaptation of step 1 in M.R.I. acquisition which is applying a slice selection gradient at the same time as the Rf excitation pulse. The position along the gradient determines resonance between the Larmor frequency and the matching Rf pulse denoted as f_0 . Modified from image found in an article of the “Journal of Cardiovascular Magnetic Resonance” [65]

The second step requires the application of a phase encoding gradient, represented as G_p . The rotation of protons will vary along the gradient which helps determine the desired

signals within the selected slice. Signal strengths from protons will either decrease or increase relative to their position along the gradient as their locations move away from the resonating frequency slice [65].

Finally, the third step requires the application of a frequency encoding gradient, represented as G_F . It is applied in directions that make right angles with the B_0 field and also causes protons to rotate at frequencies determined by their location along the gradient field.

In summary, three separate magnetic fields are produced in different steps in order to obtain an MR signal in 3-dimensions along a plane that is transaxial to the B_0 field. This ability to acquire data from any desired slice within the patient is a main reason for M.R.I. superiority with regards to cardiovascular data collection.

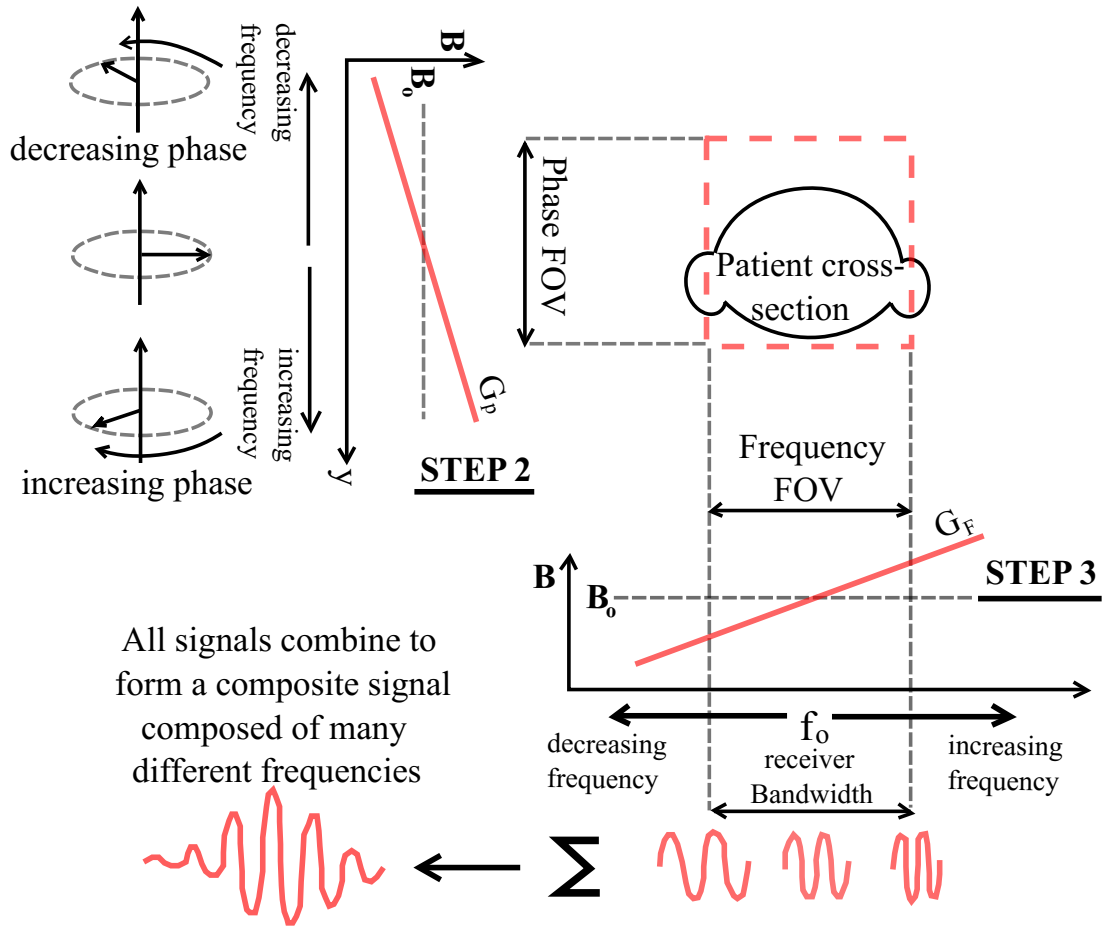


Figure 3.14: Adaptation of step 2 and 3 of M.R.I. acquisition. Step 2 involves a phase-encoding gradient G_p that causes phase shifts. Step 3 is the application of a frequency encoding gradient G_F that determines the Larmor frequency according to the desired position. Modified from image found in an article of the “Journal of Cardiovascular Magnetic Resonance” [65]

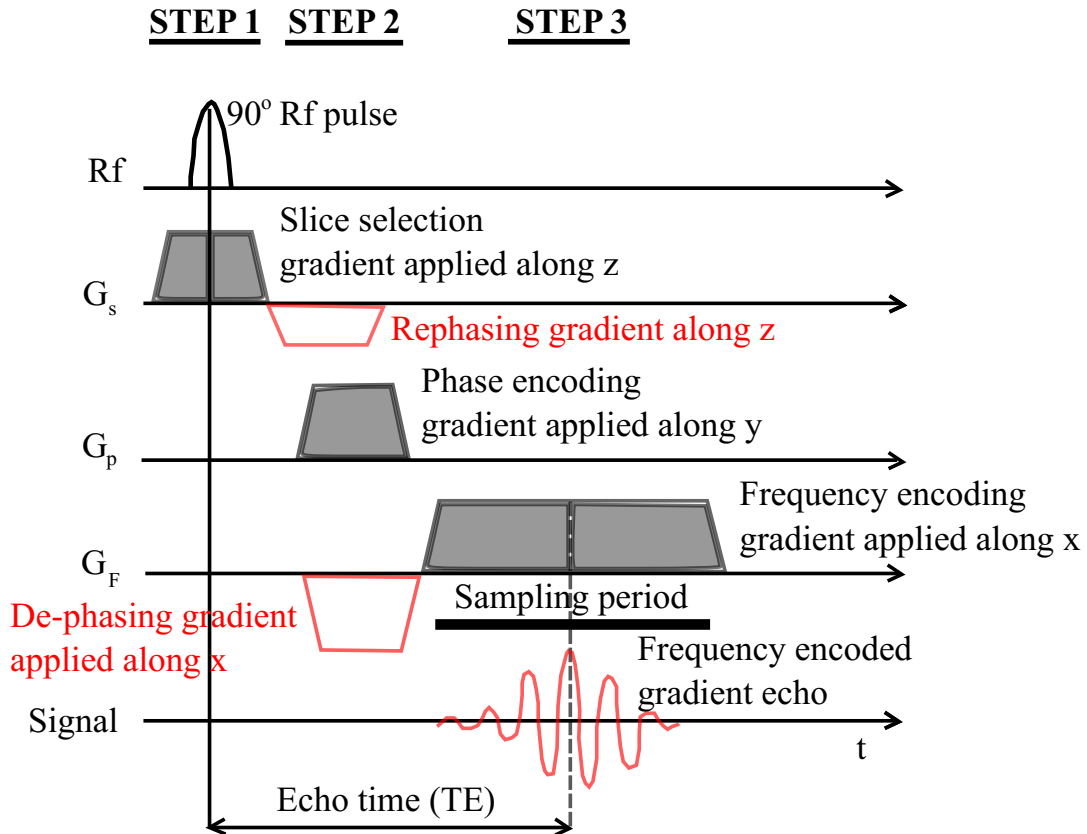


Figure 3.15: Adaptation of the pulse sequence diagram that shows the timing of the Rf and gradient pulses. This process ensures the echo signal will be at its strongest during acquisition. Modified from image found in an article of the “Journal of Cardiovascular Magnetic Resonance” [65]

3.2.4. Repetition Time

To construct an image from the acquisition data, a mathematical tool commonly known as Fourier transform is used. This method breaks down the MR signals into its different frequency components which can be used to map the location of molecules relative to their signal strength [65]. Since Fourier transform requires the signal to change over time, multiple signal echoes are repeated with different phase-encoding gradients that increase in equal increments known as TR (repetition time). Repetition time determines the speed of image acquisitions and which affects contrast quality of the image. The amount of phase encoding steps used, denoted as N_p , will determine spatial resolution and is often limited by acquisition time [65].

$$\text{Image acquisition time} = TR * N_p$$

Spin echo pulse sequences make use of a flip angle that is fixed at 90° . Gradient echo pulse sequences have the benefit of controlling the T1 and T2 relaxation times on the signal with not only repetition and echo times but also with the flip angle used. Cardiac imaging pulse sequences are synchronized with the patient's heart rate which therefore determines repetition time [65]. M.R.I. has its benefits over other cardiovascular data collecting methods but has its own limitations that have room for improvement. Since cardiovascular flow happens at such a rapid rate, M.R.I. readings cannot be acquisitioned in real time. The acquisitions captured for this dissertation represented the average of 30 complete cardiovascular cycles. An M.R.I. image must be taken in only a few tens of milliseconds to limit motion during acquisition which limits the number of encoding

steps and repetition time that affects spatial resolution. In order to achieve adequate image quality, multiple MR signals are acquired over many heart beats which are synchronized to the same instance of the R wave of the patients E.C.G. signal [65].

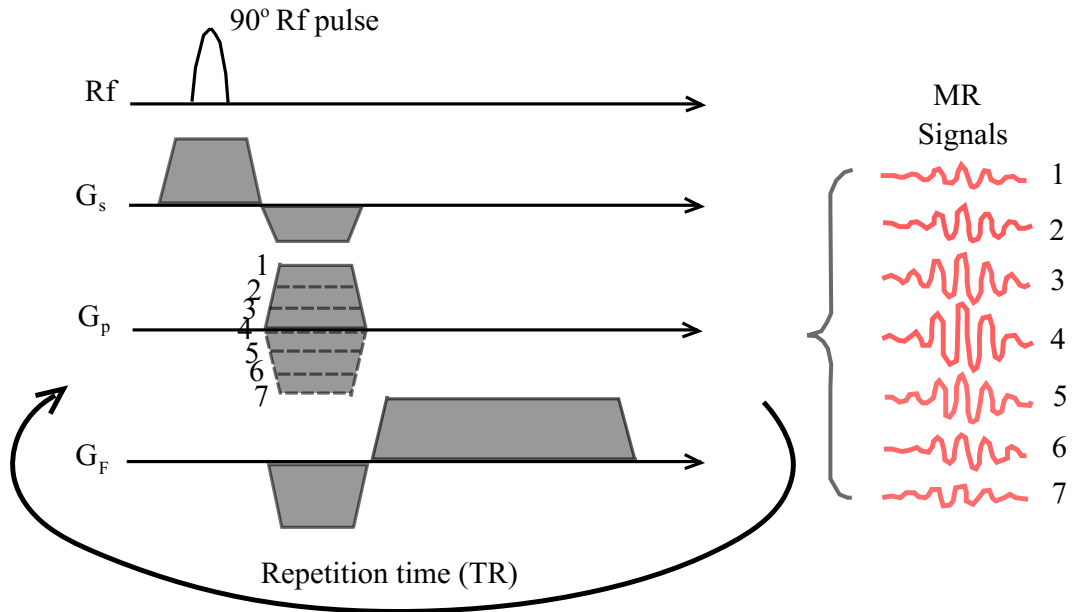


Figure 3.16: Adaptation of phase encoding steps and repetition time. The pulse sequence is repeated with incremental changes in the phase encoding gradient which allows the use of Fourier transform. Modified from image found in an article of the “Journal of Cardiovascular Magnetic Resonance” [65]

3.2.5. Flow Velocity Mapping

Flow velocity mapping is the term used when assessing blood flow patterns which is obtained using gradient echo pulse sequences. In order to acquire images rapidly, a single shot technique is used known as fast spoiled gradient echo pulse sequences which is the best method to observe regurgitation jets. Since blood flow is too rapid to rely on a second pulse to re-phase proton spins, two gradient fields of opposite signs are applied along the same direction known as the bipolar gradient pulse pair [68]. The differences between blood phases and the phases of stationary tissue help determine the velocity of the moving blood which appears as flow voids. Reducing echo time below 3.6 ms is a technique commonly used to reduce flow-related losses in signal [68].

3.3.1. M.R.I. Parameters for the MaxTron System



Figure 3.17: The system within the M.R.I. scanner

M.R.I. data offers many forms of measurement from which the focus of this dissertation was drawn towards velocity fields and particle trace mapping. A few examples of hemodynamic quantifications made possible by M.R.I. acquisitions are peak velocity, net flow, regurgitant fraction, wall shear stress, pressure difference maps, viscous energy and flow displacement [69]. All experimentation involving M.R.I. was made possible by the contributions of Dr. Julio Garcia and the Foothills Medical Center in Calgary. Much care was taken towards preserving the integrity of all equipment being used. Reservoirs for the MaxTron system were kept at a distance of about 2 m from the scanner within the M.R.I. room. This was not ideal for safety reasons but helped keep pressure levels of the system calibrated. The M.R.I. scanner used was a Prisma 3T system (Siemens: Munich, Germany) with spatial resolution of $2.5 \times 2.5 \times 2.5 \text{ mm}^3$ and temporal resolution of 30-40

ms. Acquisition times were between 3 and 16 min depending on amount of severities being tested. The method for acquisition uses 3-dimensional phase contrasting (P.C.-M.R.I.) with respect to time and delivers 3- directional velocity encoding and is termed 4D flow M.R.I. [70]. The range for VENC (velocity encoding) was typically -150 to 150(cm/s). Eight phase encoding steps were used with a repetition time of 5.06 ms and echo time of 2.36 ms. A Gadolinium based contrast agent named Gadavist (Bayer: Leverkusen, Germany) was added into the water ($1\text{ }^{cc}/litre$) during circulation which helped with the visualization of the flow. A low flip angle of 7° was used for fast acquisition gradient echo pulse sequencing. Data pre-processing is a step that involves corrections in the form of segmenting the cardiovascular geometry which helped alleviate acquisition problems that could affect flow quantification and visualisation. Main sources of errors that can occur within the acquired data are the presence of eddy currents, gradient field effects and phase wraps that can produce velocity aliasing. Aliasing happens when velocities exceed the pre-determined velocity range limits of the acquisition [71].

Both standard deviation and noise filters were applied to the M.R.I. data once obtained. Matlab (Mathworks; Natick, MA, U.S.A.) versions of the data and files intended for a program named Enight (Siemens; Munich, Germany) were then created. The files uploaded to the Enight software program made visualization of the flow possible along with the possibility to create planes at any desired location in the data set.

Chapter 4

4 Results

4.1.1. Introduction

The compatibility of the system when introduced to an M.R.I. environment will be discussed first. Many preparations needed to be done in order to have back-up components in the case of failure. M.R.I. usage for experimentation in this case was restricted to hours that the scanner was not being used for clinical purposes, which were limited. First attempts were done using the linear motor to activate both sides of the heart which was limited to 50 bpm. When used for one side only, the system could attain 70 bpm for the length of acquisition time needed which was between 3 and 16 min. The system was validated by pressures recorded using a fibre optic pressure sensor (FOP-M260-10 sensor with FPI-HR model, FISO Technologies Inc.; Quebec, Canada) with an accuracy of ± 3 mmHg. Flow rate was measured on site using more unconventional methods due to no metal components allowed in proximity and were on average around 1.5 L per min. This flow rate is considered low but was sufficient to prove the concept of this system. The pressure waveforms presented below were obtained in the aorta, left ventricle, right ventricle and pulmonary artery within the L.C.F.D. but not on site during M.R.I. experimentation due to the restriction of metallic components.

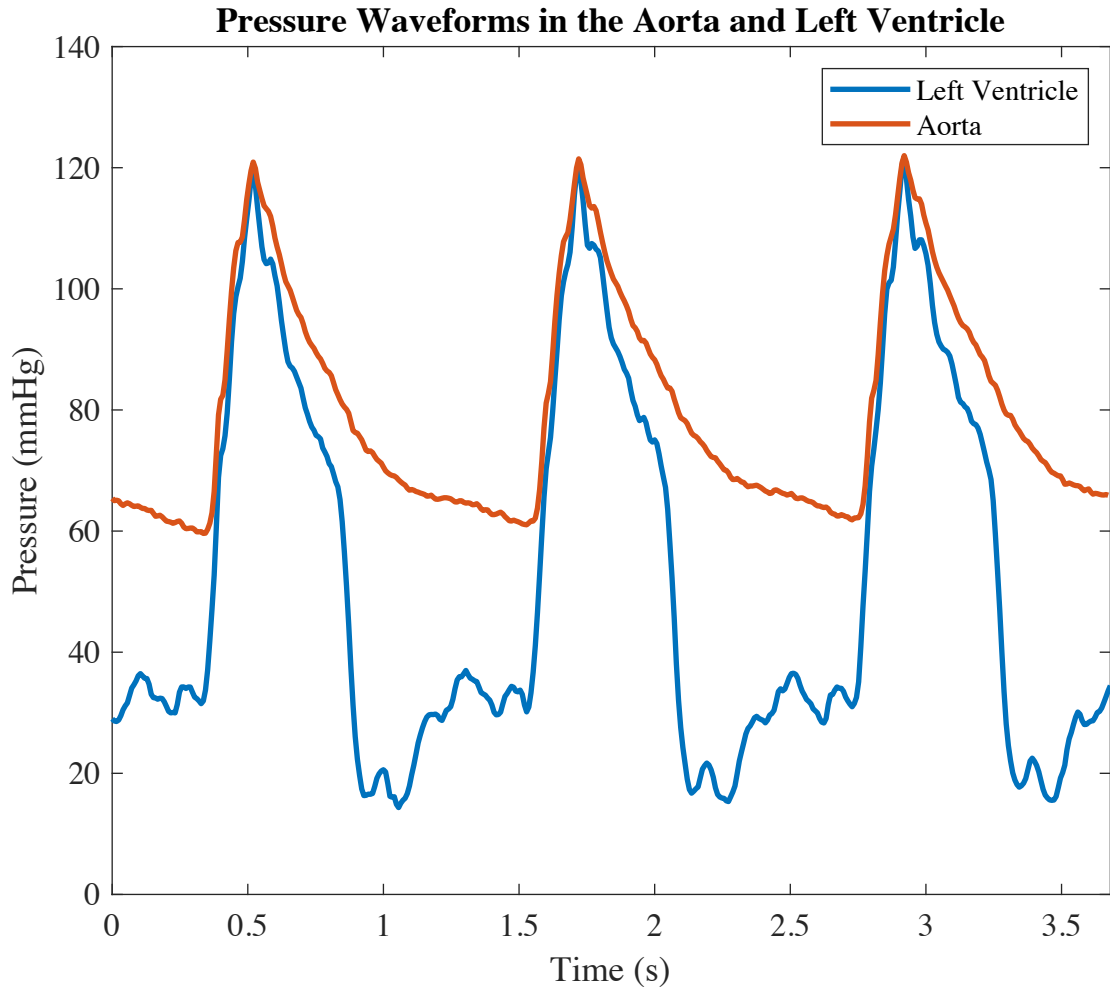


Figure 4.1: Pressure waveforms for both the aorta and left ventricle which were obtained simultaneously at 50 bpm

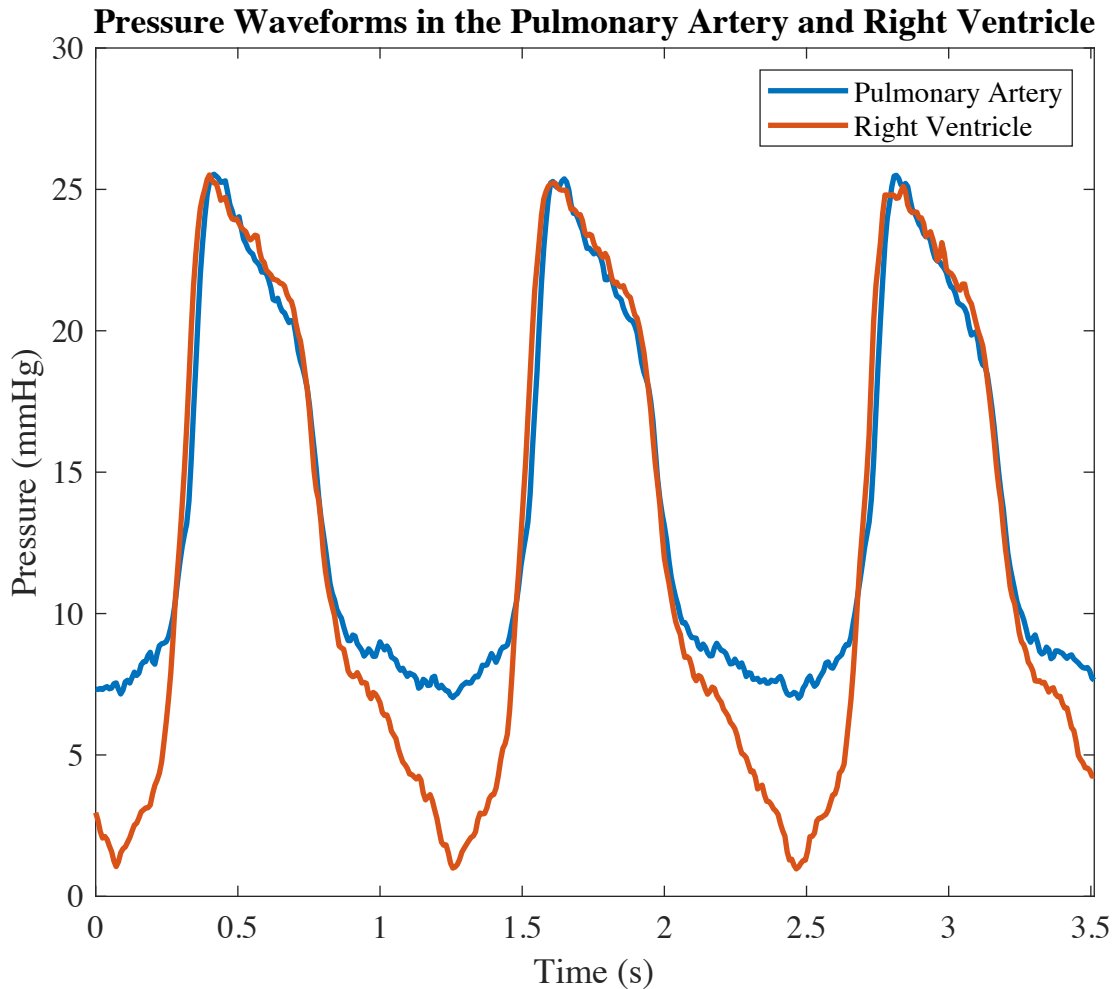


Figure 4.2: Pressure readings for both the pulmonary artery and right ventricle which were taken simultaneously at 50 bpm

The above results for the left and right side of the system were taken simultaneously at 50 bpm. One can notice that amplitudes reach their targeted values and waveforms are smooth. They have a slightly reversed effect with regards to drops compared to the targeted right side pressure waveforms but represent a great step in the right direction. The exit tubes of the pulmonary artery were replaced with smaller diameter rubber tubing and valves that could regulate the capillary resistance in a repeatable and accurate way.

4.1.2. M.R.I. Compatibility

One main consideration was signal reception throughout M.R.I. experimentation. All the components of the system proved to be M.R.I. compatible, but certain measures were taken to improve the signal obtained during acquisitions. Water bottles were placed in and around the system to capture Rf energy that would usually be absorbed within human patients. Rf receiver coils used to collect signals are basic resistance-capacitance tuned antennas that have a saturation limit. Without the addition of water bottles Rf energy is reflected and captured in the coils as a measured signal. This creates noise in the acquired data and could potentially harm the coils. The following figure demonstrates the differences between a high and low signal to noise ratio along with replacement valve considerations. The gap seen in the mitral position in the setup on the left side of the heart contained M.R.I. compatible metal whereas the setup on the right housed a Lifelike bi-leaflet mitral valve and did not create the same lack of signal in that area. When inside the M.R.I. scanner, the system is strapped to the table using a phase-array body receiver coil that mounts over the system and applies downward pressure. This was further cause for loss of signal during acquisitions due to interference caused by the close proximity of the coil. This phenomenon can also be noticed in the right image above the aorta in the following figure. It is also imperative that the heart components and support structures move as little as possible during ventricular activation which can cause a tracing effect seen in the right image within the aorta curvature.

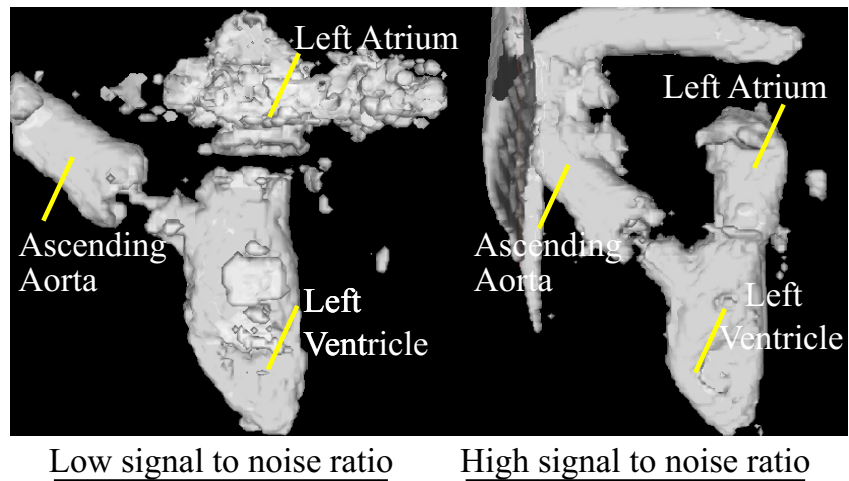


Figure 4.3: Differences in signal reception during acquisitions. Left side of the figure houses two bio-prosthetic valves containing metal components whereas the right side of the figure has a bi-leaflet Lifelike valve in the mitral position and therefore obtained a clearer signal without any gap

4.1.3. M.R.I. 3-Dimensional Results

Proof of concept was achieved and repeated many times to test many severities of aortic regurgitation. From the Ensign software program, 3D visualization of the results is made possible. Planes that are created anywhere along the setup can be used to quantify the flow velocities, demonstrate the trajectories taken by particles within the flow and color code the velocities with respect to magnitudes. Another feature easily applied to the data is a particle trace image that shows the total trajectory of all the particles being observed in the flow. This allows quick visualisation of turbulence and vortex formations

involved in the complete cardiac cycle. The following figure demonstrates 3-dimensional results from a front point of view. The left figure demonstrates the diastolic phase and the middle figure depicts the systolic phase. The figure on the right is a particle trace image of the path taken of selected particles during one cardiac cycle.

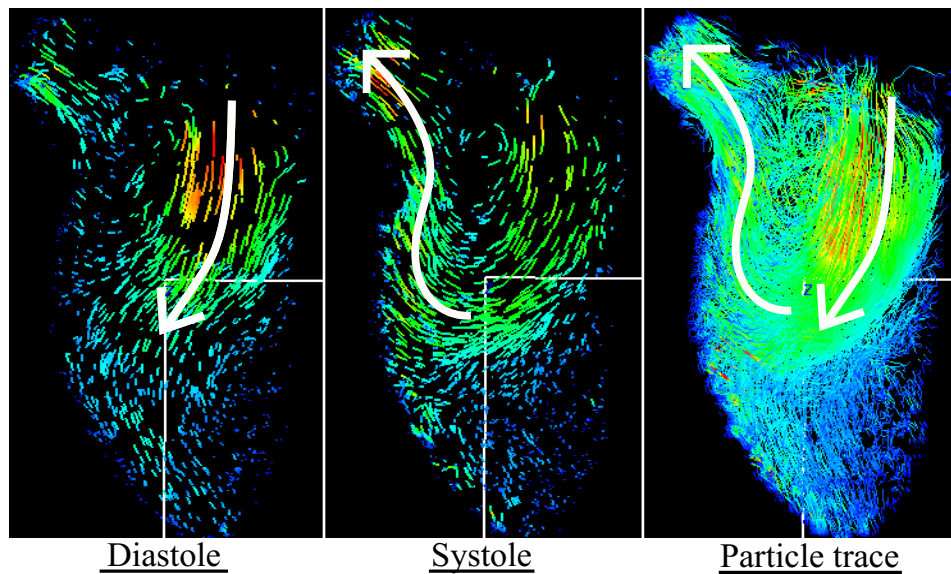


Figure 4.4: Three-dimensional pathline results from M.R.I. acquisitions. Left figure represents the diastole phase, middle figure represents the systole phase and the right figure demonstrates a particle tracing image throughout the entire cardiac cycle

One important observation about the above results is the lack of circulation in the bottom half of the ventricle. This was a result of the contact area available with the pusher activation. This phenomenon is however a consequence of other pathologies that merit further studies as well. Some examples could be interventricular and intraventricular dyssynchrony. Interventricular dyssynchrony is a disease where the left ventricle contraction is not synchronized with the right ventricle. Intraventricular dyssynchrony is

a disease where the contraction of segments of the left ventricle is delayed. The cardiac output remains the same between patients with or without this disease however patients with intraventricular dyssynchrony have increased end-diastolic volumes due to the shortened filling time [72]. Another example is a disease called giant left atrium disease which affects the compression of the left ventricle. The oversized left atrium compresses the posterobasal wall of the left ventricle which bends it against the septal wall that separates the right and left ventricles [73]. These diseases could increase the potential for stagnation zones in the left ventricle during the cardiac cycle and can be simulated with the system.

4.1.4. 2-Dimensional Results

Although 3-dimensional data provides great visualization of flow characteristics, quantification for the time being is better achieved using 2-dimensional slices of the 3-dimensional data. The post processing for 3-dimensional data requires additional efforts that were not permitted during the extent of this project therefore observations will be made using 2-dimensional analysis of both pathlines and velocity fields. Selections were made throughout the numerous data sets that highlight the changes in flow when severities of aortic regurgitation were induced in a progressive order. Despite an immense learning curve, M.R.I. data was retrieved in 3-dimensions from which flow disturbances caused by aortic regurgitation can be visualized. The 2-dimensional view of the velocity fields that will follow are for the moment easier to present and comprehend when not animated.

*Mitral Valve: Mechanical, Aortic Valve: Biocor bio-tissue, 3 leaflet regurgitation
 R.O.A.(Regurgitant Orifice Area): 0.00 cm²

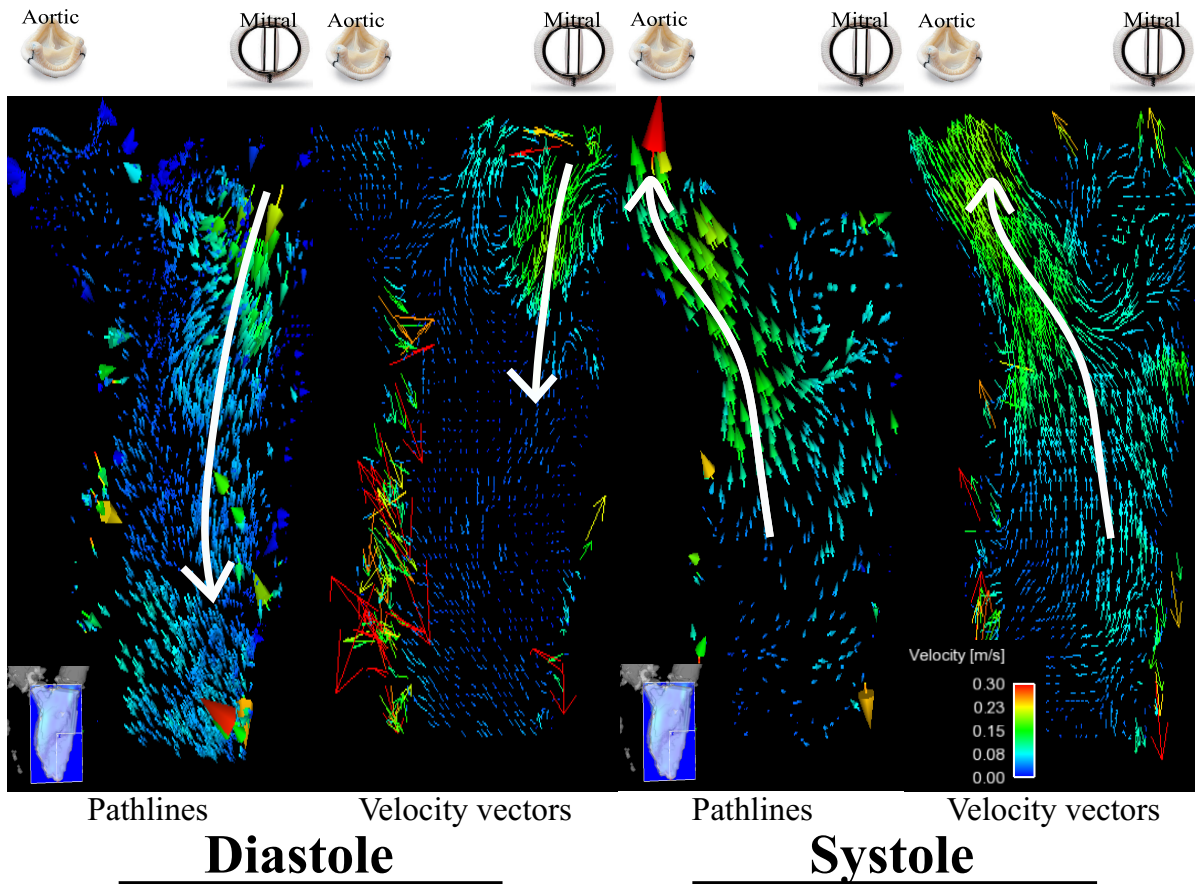


Figure 4.5: M.R.I. acquisition results of a healthy patient simulated case

The above figure demonstrates one plane within the heart of the system as depicted by the pictogram in the lower left hand corners. At the top of each image, the heart valve used for that location is also represented by a pictogram. The two images on the left are still shots of both the pathlines and the velocity vectors during diastole of a healthy heart. For the sake of clarity while presenting these results the amount of vectors representing the velocity field was reduced to 40% density and the pathlines are represented by arrow

heads that match their magnitudes respectively. The two images on the right side of the figure represent the pathlines and velocity vectors of the systolic phase of the same cardiac cycle acquisition. The above figure was the first results obtained with the system and is referred to as setup 1. A mechanical heart valve was used for the mitral location and a bio-tissue heart valve was used for the aortic location. These preliminary readings were scattered with noise which were associated to the learning curve as can be noticed in the second image of the above figure. Observations of the mitral inflow which is directed toward the tip of the apex at the bottom of the left ventricle can be easily visualized along with fluid interactions with the ventricle walls represented by the two images on the left. Very clear pathlines of fluid leaving the ventricle towards the aortic valve can also be visualised in both left images. The uniqueness of the MaxTron system is that from the same M.R.I. results, any plane in the system during the cardiac cycle can be analysed which till now has not been a possibility on any *in vitro* system of this caliber. To keep this dissertation concise only a few examples of the limitless possibilities of the system will be presented.

ventricle and are also depicted in the pictogram. These views of the cardiac cycle are rarely observed and offer a clearer image of flow characteristics from a different perspective.

4.1.5. Aortic Regurgitation Simulation

A few iterations were brought to the system which allowed the simulation of aortic regurgitation. Although many lessons had already been learnt, there were still many stepping stones of apprenticeship conquered during the preceding iterations. Insight to the hemodynamics involved with aortic regurgitation is essential towards developing better diagnostic methods, medical devices and patient specific parameters. Throughout the testing of progressive severities of aortic regurgitation many complications limited the consistency of the results therefore selections of a few acquisitions will be presented which fulfill the objective of discovering the feasibility of the system. The following results demonstrate mild aortic regurgitation.

*Mitral Valve: Lifelike bio-tissue, Aortic Valve: Biocor bio-tissue, 3 leaflet regurgitation
 R.O.A.(Regurgitant Orifice Area): 0.125 cm²

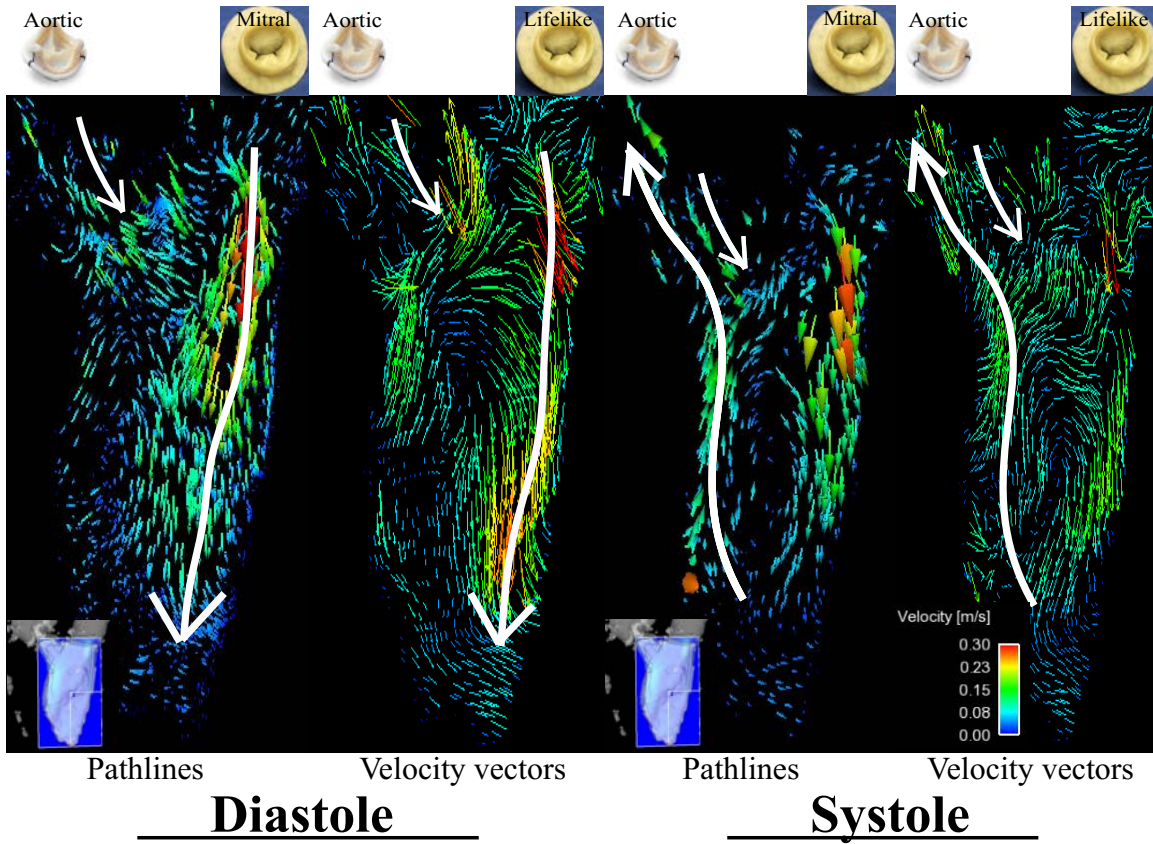


Figure 4.7: M.R.I. acquisitions of a mild aortic regurgitation simulation

A quick observation in the above figure can be made about the beginning of flow disturbance during each phase. During diastole, the regurgitant jet can be noticed colliding with mitral inflow causing slight disruptions. The same regurgitant jet persists during systole. The cause for this was the Lifelike heart valve chosen for the mitral location during this iteration. The Lifelike valve offered physiological mitral inflow but due to the fact that it was not properly tethered made it not close efficiently during the

affecting only one leaflet which will be presented below. The direction of the regurgitant jet along with the size of the leaking orifice both plays a role in the increased disturbance of the flow.

*Mitral Valve: Lifelike bio-tissue, Aortic Valve: Biocor bio-tissue, 1 leaflet regurgitation
 R.O.A.(Regurgitant Orifice Area): 0.496 cm^2

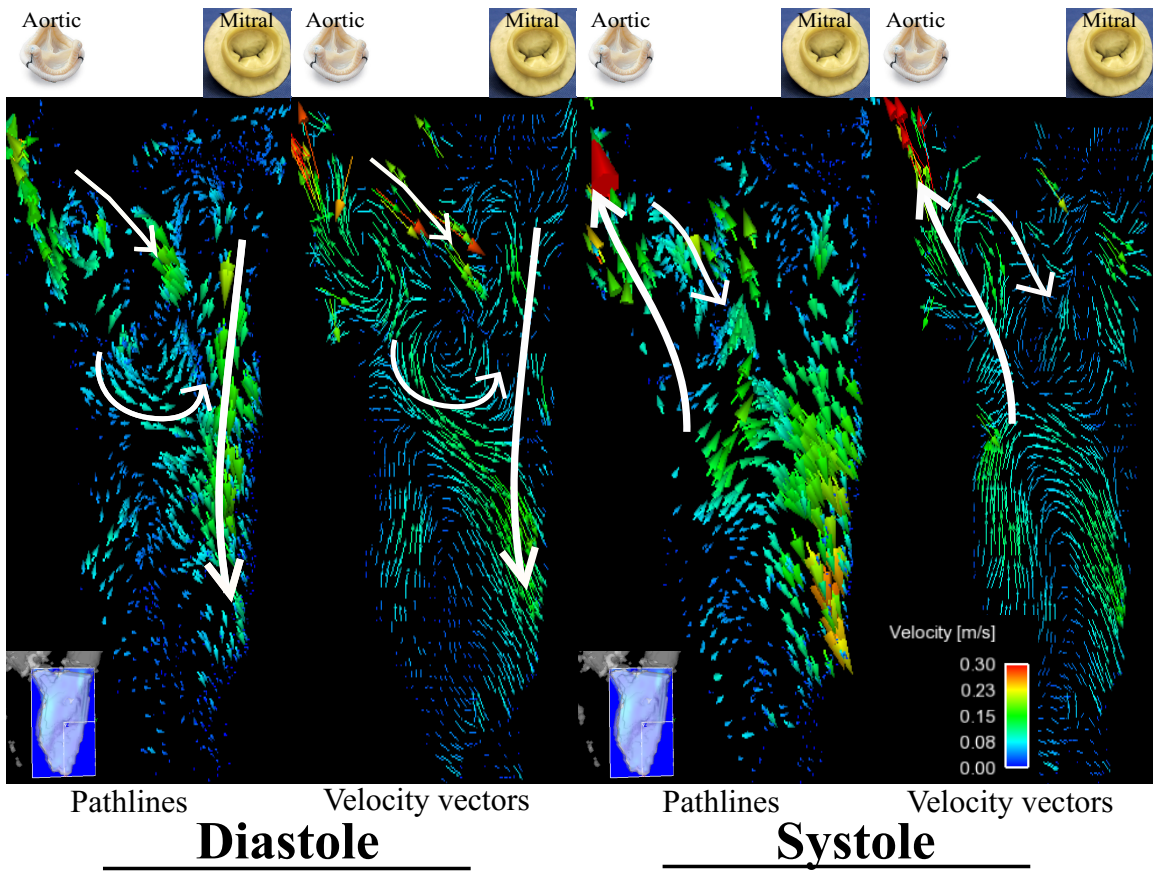


Figure 4.9: M.R.I. acquisition results of severe aortic regurgitation simulation

An increase in flow disturbance proportional to the increase in R.O.A. can be noticed in the above figure. Although the cardiac cycle is difficult to distinguish with this iteration

there is still an opportunity to gain insight. One important observation is how regurgitant mitral inflow seems to diminish in the presence of a stronger aortic regurgitant jet.

4.1.6. Mitral Valve Orientation

An observation was made throughout experiment iterations where the mitral valve had been placed at a different angle as opposed to its anatomical placement which led to the mitral inflow jet being aimed towards the septal wall instead of the posterior wall of the left ventricle. This phenomenon when mixed with different severities of aortic regurgitation had some interesting outcomes that are worth noticing. The incoming aortic regurgitant jet collides with the misaligned mitral inflow jet in such a way that the flow disturbance is minimized as can be noticed in the following figure.

*Mitral Valve: Biocor bio-tissue, Aortic Valve: Biocor bio-tissue, 1 leaflet regurgitation
R.O.A.(Regurgitation Orifice Area): 0.496 cm²

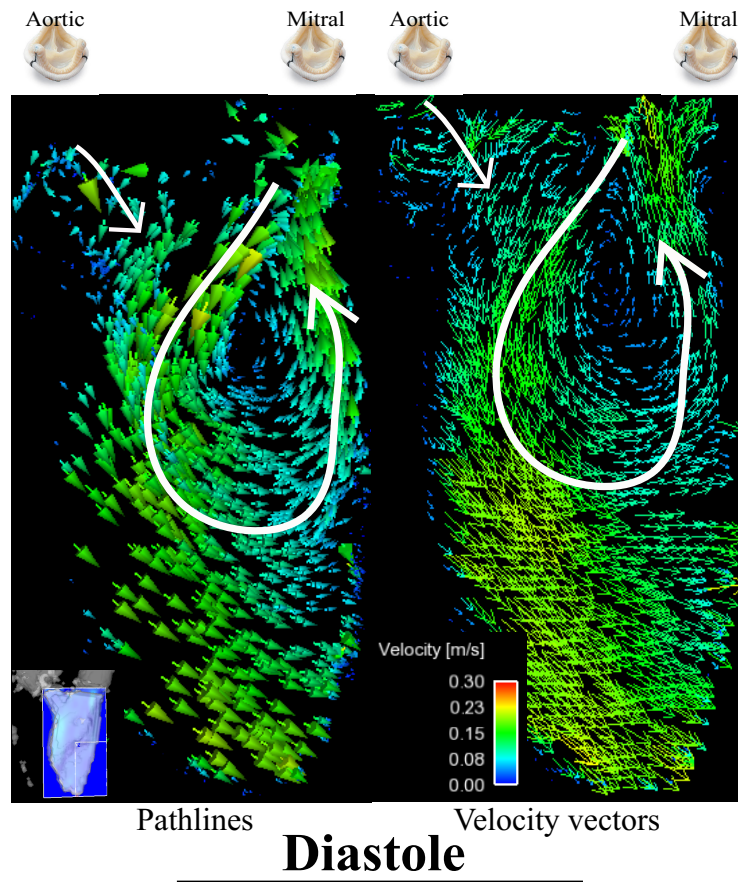


Figure 4.10: Mitral orientation change M.R.I. acquisition results for severe aortic regurgitation simulation

Due to minimized acquisition time the cycle was not completely registered but the effect of a reversed vortex can be noticed in the diastolic results of both pathlines and velocity vectors. The angle at which both incoming jets are placed optimizes an immediate mixture of the jets into one with minimal disturbance leading to a near laminar flow. The flow had a tendency to remain the same despite the progressions of increasing severities of aortic regurgitation. Flow patterns may behave in reverse compared to physiological

hemodynamics with regards to flow displacement but these findings merit further investigation. An example that comes to mind is if a patient was in need of both an aortic and mitral heart valve replacement surgery, one option depending on the patient's age and risk factors could be to only replace the mitral heart valve and have it orientated in such a way to minimize the need to repair the aortic heart valve. This could prove beneficial for high risk or elderly patients that have lower chances of surviving dangerous surgeries.

Chapter 5

5 Conclusion

5.1.1. Discussion

A major contribution from this experiment towards improving cardiovascular research was the durability of the heart components. The 3D printed silicone hearts produced by the University of Zurich have a life span of approximately 30 min [56]. The heart components produced in the L.C.F.D. laboratories have proven that they can be used for a much longer duration and the same heart cavities have been used throughout this research. The main focus of the project however was M.R.I. compatibility which shall now be further discussed. The production of heart components was proven possible through the use of Ninjaflex 3D printing filament. The implementation of an interchangeable 3D printed support structure was proven effective to house any type of structural support with the ultimate goal of patient specific representation. This gives the MaxTron heart simulator system unlimited potential to expand research capability towards a multitude of options. This includes extending the amount of pathologies covered in cardiovascular related fields along with other organs that might interact with these pathologies. With the advancements in tissue engineering, enhanced heart components will represent the ultimate addition to these types of simulators. Dual material 3D printed heart components will soon have the potential to accurately distinguish mechanical properties of natural heart components. The M.R.I. compatibility of the simulator and all its components was therefore achieved and validated with the pressure waveforms. Aortic regurgitation was simulated through progressive states of

severities and even though the results are rudimentary, they represent a positive step towards bettering cardiovascular fluid dynamic research. Through the course of experimentation it was also noticed that mitral inflow orientation can have a positive effect on flow disturbance caused by increasing severities of aortic regurgitation.

One of the biggest limitations throughout these experiments was the low flow rate. Future iterations of these heart simulators are presently being worked on at the L.C.F.D. The system will definitely benefit from the addition of a soft robotic or origami activation system to increase the flow rate and minimize components needed for activation of the circulatory system. Attempts are being made to incorporate soft robotic tubing in a helical fashion within the ventricle walls which when activated will create a more realistic replica of how the heart actually contracts its myocardial muscle fibres to produce circulation [74].



Figure 5.1: Adaptation of the theoretical placement of soft robotics inside heart component walls enabling realistic compression of the heart. Modified from image found on the “Soft Robotics Toolkit” website [74]

A brief mention that there are many other different tasks that the simulator can accomplish. One field of research that is increasing in importance is the effects of zero gravity on the cardiovascular circulatory system. Space flight involves many unanswered questions when cardiovascular functionality is concerned. Current studies performed in a zero gravity environment show significant cardiovascular changes in endothelial cells that line up the vasculatory network of arteries and heart chambers [75] which could potentially be simulated with the MaxTron system. Other future advancements in cardiovascular research involve many companies like I.B.M., Apple and Google which

are investing in developing and adapting artificial intelligence that could possibly assist in diagnostics. A.I. has the advantage of being able to assess large amounts of data [76].

5.1.2. Limitations

The most important improvement to the acquisitions would be to solve the trigger issues that start the acquisition at a desired instance. The problem of trigger signal reception was evasive because the signal was being sent properly with the correct impedance however the M.R.I. scanner was not detecting the signal for some unknown reason. Water was used for these experiments but future use of a water-glycerol solution would prove more physiologically correct. Flow rate was low which was due to the linear motor limitations. Other limitations included pusher contact area with respect to the ventricle compressions which could benefit from further iterations with the goal of distributing compression more evenly and starting from the apex of the ventricle working upward. Adapting the system so the torso casing could be filled completely with liquid would help the signal reception for M.R.I. readings and would add the availability to the system to house Lifelike heart components made from tissue engineered materials that need to be constantly submerged in liquid. A quicker connection and disconnection method could further user-friendliness of the system and would help reduce acquisition times.

Research in this field is very gratifying due to the severity and abundance of cardiovascular diseases within the global population. Medical device testing, medical education and cardiovascular fluid dynamics will continue to benefit from the advancements in medical simulators which increase competency of device designers and physicians along with fulfilling the ultimate goal of improving overall patient safety.

References

- [1] Fine J.M., Waite L, *Applied Biofluid Mechanics*, 1st ed.: McGraw-Hill Education, 2007.
- [2] Bianco C, *How your heart works.*, 2004.
- [3] Texas Heart Institute. (2020, February) Texas Heart. [Online]. <https://www.texasheart.org/heart-health/heart-information-center/topics/the-heart-valves/>
- [4] Fisher J, Ingham E, Korossis S.A., "Cardiac valve replacement: A bioengineering approach," *Bio-medical materials and engineering*, vol. 10, no. 2, pp. 83-124, 2000.
- [5] Chaux A, Gray R.J., Woo Y.R., De Robertis M, Williams F.P., Matloff J.M., Yoganathan A.P., "Bileaflet, tilting disc and porcine aortic valve substitutes: In vitro hydrodynamic characteristics," *Journal of the American College of Cardiology*, vol. 2 Part 1, no. 3, pp. 313-320, 1984.
- [6] Wang J.J., Mitchell J.R., "Expanding application of the Wiggers diagram to teach cardiovascular physiology," *Advances in Physiology Education*, vol. 38, no. 2, pp. 170-175, 2014.
- [7] World Health Organization. (2020, February) who. [Online]. https://www.who.int/health-topics/cardiovascular-diseases/#tab=tab_1
- [8] Smith E.R., "The Canadian heart health strategy and action plan," *The Canadian journal of cardiology*, vol. 25, no. 8, p. p.451, 2009.
- [9] American Heart Association. (2020, March) Heart. [Online]. <https://www.heart.org/en/health-topics/heart-valve-problems-and-disease/understanding-your-heart-valve-treatment-options/options-for-heart-valve-replacement>
- [10] Komninou M.A., Badria A.F., Korossis S, Koutsoukos P, Mavrilas D, D'Alessandro C.C., "Calcification assessment of bioprosthetic heart valve using an improved in vitro model," *IEEE Transactions on Biomedical Engineering*, p. 1, 2020.
- [11] Evans J.C., Levy D, Larson M.G., Freed L.A., Fuller D.L., Lehman B, Benjamin E.J., Singh J.P., "Prevalence and clinical determinants of mitral, tricuspid, and aortic regurgitation (the Framingham Heart Study)," *The American Journal of Cardiology*, vol. 83, no. 6, pp. 897-902, 1999.
- [12] Raghav V, Condado J.F., Midha P.A., Kumar G, Yoganathan A.P., Okafor I, "Aortic regurgitation generates a kinematic obstruction which hinders left ventricular filling," *Annals of Biomedical Engineering*, vol. 45, no. 5, pp. 1305-1314, 2017.

- [13] Ojha M, Johnston K.W., Harlal A, "Vena cava filter performance based on hemodynamics and reported thrombosis and pulmonary embolism patterns," *Journal of Vascular and Interventional Radiology*, vol. 18, no. 1, pp. 103-115, 2007.
- [14] Klabunde R., *Cardiovascular Physiology Concepts.*: Lippincott Williams & Wilkins, 2011.
- [15] Jones D, McLaurin L.P., Grossman W, "Wall stress and patterns of hypertrophy in the human left ventricle," *The Journal of Clinical Investigation*, vol. 56, no. 1, pp. 56-64, 1975.
- [16] Verrier E.D., Stout K.K., "Acute valvular regurgitation," *Circulation*, vol. 119, no. 25, pp. 3232-3241, 2009.
- [17] Duan B, "State of the art review of 3D bioprinting for cardiovascular tissue engineering," *Annals of Biomedical Engineering*, vol. 45, no. 1, pp. 195-209, 2017.
- [18] Bloomfield P, "Choice of heart valve prosthesis," *Heart*, vol. 87, no. 6, pp. 583-589, 2002.
- [19] Maddox T.M., Tillquist M.N., "Cardiac crossroads: Deciding between mechanical or bioprosthetic heart valve replacement," *Patient Preference and Adherence*, vol. 5, p. 91, 2011.
- [20] the Drs Wolfson. (2020, May) the drs wolfson. [Online].
<https://thedrswolfson.com/mechanical-heart-valve/>
- [21] Shuren J, Faris O, "An FDA viewpoint on unique considerations for medical device clinical trials," *New England Journal of Medicine*, vol. 376, no. 14, pp. 1350-1357, 2017.
- [22] Hon R.T., Yoganathan A.P., Marquez S, "Comparative hydrodynamic evaluation of bioprosthetic heart valves," *The Journal of Heart Valve Disease*, vol. 10, no. 6, pp. 802-811, 2001.
- [23] Amin A, Tu J, Echenique A, Winokur R.S., Miller Z.A., "Simulation-based training for interventional radiology and opportunities for improving the educational paradigm," *Techniques in Vascular and Interventional Radiology*, vol. 22, no. 1, pp. 35-40, 2019.
- [24] Vanderbilt University Medical Center. (2020, March) News Vanderbilt University Medical Center. [Online]. <https://news.vumc.org/2016/09/01/new-simulation-tool-helps-sharpen-heart-surgery-skills/>
- [25] Olivieri L.J., Su L, Krieger A, Alfares F, Thabit O, Marshall M.B., Yoo S.J., Kim P.C., Jonas R.A., Nath D.S., Costello J.P., "Incorporating three-dimensional printing into a simulation-based congenital heart disease and critical care training curriculum for resident physicians," *Congenital Heart Disease*, vol. 10, no. 2, pp. 185-190, 2015.
- [26] Kelil T, Cheeum M.K., Goncalves A, Di Carli M.F., Rybicki F.J., Steigner M, Mitsouras D,

- Blankstein R, Ripley B, "3D printing based on cardiac CT assists anatomic visualization prior to transcatheter aortic valve replacement," *Journal of Cardiovascular Computed Tomography*, vol. 10, no. 1, pp. 28-36, 2016.
- [27] Figueroa C.A., Taylor C.A., "Patient-specific modeling of cardiovascular mechanics," *Annual Review of Biomedical Engineering*, vol. 11, pp. 109-134, 2009.
- [28] Di Labbio G, "On left ventricle fluid dynamics associated with progressive chronic aortic regurgitation," Concordia University, Doctoral Dissertation 2019.
- [29] Adrian R, Squires K, Chaliki H, Belohlavek M, Westerdale J.C., "Effects of bileaflet mechanical mitral valve rotational orientation on left ventricular flow conditions," *The Open Cardiovascular Medicine Journal*, vol. 9, p. 62, 2015.
- [30] Robicsek F, "Leonardo Da Vinci and the sinuses of Valsalva," *The Annals of Thoracic Surgery*, vol. 52, no. 2, pp. 328-335, 1991.
- [31] Wade J.D., Taylor D.E.M., "Pattern of blood flow within the heart: A stable system," *Cardiovascular Research*, vol. 7, no. 1, pp. 14-21, Jan 1973.
- [32] Yokote Y, Takamoto S, Kyo S, Ueda K, Asano H, Namekawa K, Kasai C, Kondo Y, Koyano A, Omoto R, "The development of real-time two-dimensional Doppler echocardiography and its clinical significance in acquired valvular diseases," *Japanese Heart Journal*, vol. 25, no. 3, pp. 325-340, 1984.
- [33] Izuma S, Okamoto M, Kinoshita N, Asonuma H, Nakagawa H, Yamamoto K, Takamiya M, Sakakibara H, Nimura Y, Miyatake K, "Semiquantitative grading of severity of mitral regurgitation by real-time two-dimensional Doppler flow imaging technique," *Journal of the American College of Cardiology*, vol. 7, no. 1, pp. 82-88, 1986.
- [34] Poelma C, "Ultrasound imaging velocimetry: a review," *Experiments in fluids*, vol. 58, no. 1, p. 3, 2017.
- [35] Nayler G.L., Klipstein R.H., Underwood S.R., Rees R.S., Longmore D.B., Firmin D.N., "In vivo validation of MR velocity imaging," *Journal of Computer Assisted Tomography*, vol. 11, no. 5, pp. 751-756, 1987.
- [36] Kilner P.J., Wood N.B., Underwood S.R., Firmin D.N., Yang G.Z., "Computation of flow pressure fields from magnetic resonance velocity mapping," *Magnetic Resonance in Medicine*, vol. 36, no. 4, pp. 520-526, 1996.
- [37] Burger P, Kilner P.J., Mohiaddin R.H., Yang G.Z., "In vivo blood flow visualization with magnetic resonance imaging," *Proceedings of the 2nd conference on Visualization'91*, pp. 202-209, 1991.

- [38] Firmin D.N., Longmore D.B., Nayler G.L., "Blood flow imaging by cine magnetic resonance," *Journal of Computer Assisted Tomography*, vol. 10, no. 5, pp. 715-722, 1986.
- [39] Kilner P.J., Ebbers T, Markl M, "Comprehensive 4D velocity mapping of the heart and great vessels by cardiovascular magnetic resonance," *Journal of Cardiovascular Magnetic Resonance*, vol. 13, no. 1, 2011.
- [40] Yang G.Z., Kilner P.J., Mohiadden R.H., "Visualization of flow by vector analysis of multidirectional cine MR velocity mapping," *Journal of Computer Assisted Tomography*, vol. 18, no. 3, pp. 383-392, 1994.
- [41] Weiting D.W., "In vitro testing of heart valves: Evolution over the past 25 years," *The Annals of Thoracic Surgery*, vol. 48, no. 3, pp. S12-S13, 1989.
- [42] Talbot L, Bellhouse B.J., "The fluid mechanics of the aortic valve," *Journal of Fluid Mechanics*, vol. 35, no. 4, pp. 721-735, 1969.
- [43] Bellhouse B.J., "Fluid mechanics of a model mitral valve and left ventricle," *Cardiovascular Research*, vol. 6, no. 2, pp. 199-210, 1972.
- [44] Williams W.G., Bellhouse B.J., "Prosthetic Valve," US Patent 4,204,283, 1980.
- [45] Weiting D.W., Baehr D.A., Bard R.J., Brugger J.P., Harrison E.C., Dellsperger K.C., "Regurgitation of prosthetic heart valves: Dependence on heart rate and cardiac output," *The American Journal of Cardiology*, vol. 51, no. 2, pp. 321-328, 1983.
- [46] Chaux A, Gray R.J., Woo Y.R., De Robertis M, Williams F.P., Matloff J.M., Yoganathan A.P., "Bileaflet, tilting disc and porcine aortic valve substitutes: In vitro hydrodynamic characteristics," *Journal of the American College of Cardiology*, vol. 3, no. 2 part 1, pp. 313-320, 1984.
- [47] Woo Y.R., Sung H.W., Williams F.P., Franch R.H., Jones M, Yoganathan A.P., "In vitro hemodynamics characteristics of tissue bioprostheses in the aortic position," *The Journal of Thoracic and Cardiovascular surgery*, vol. 92, no. 2, pp. 198-209, 1986.
- [48] Yoganathan A.P., Williams F.P., Stevenson D.M., "Numerical simulation of steady turbulent flow through trileaflet aortic heart valves-2. Results on five models," *Journal of Biomechanics*, vol. 18, no. 12, pp. 909-926, 1985.
- [49] Van De Vosse F.N., Baaijens F.P.T., Stijnen J.M.A., "Influence of prosthetic mitral valve orientation on left ventricular flow," *Computers in Cardiology*, vol. 28, pp. 173-175, 2001.
- [50] Chandran K.B., Manning K.B., Bluestein D, "Towards non-thrombogenic performance of blood recirculating devices," *Annals of biomedical engineering*, vol. 38, no. 3, pp. 1236-

1256, 2010.

- [51] Delfino J.G., Sharma P, Gharib A.M., Pettigrew R.I., Oshinski J.N., "Cardiovascular magnetic resonance at 3.0 T: Current state of the art," *Journal of Cardiovascular Magnetic Resonance* , vol. 12, no. 1, p. 55, 2010.
- [52] Zhong L, Wang X.K., Zhang J.M., San Tan R, Allen J.C., Tan S.K., Kim S, Leo H.L., Su B, "Numerical simulation of patient-specific left ventricular model with both mitral and aortic valves by FSI approach," *Computer Methods and Programs in Biomedicine*, vol. 113, no. 2, pp. 474-482, 2014.
- [53] Koriyama H, Katsuki K, Masuda K, Asanuma T, Takeda Y, Sakata Y, Itatani K, Nakatani S, Stugaard M, "Energy loss in the left ventricle obtained by vector flow mapping as a new quantitative measure of severity of aortic regurgitation: a combined experimental and clinical study," *European Heart Journal-Cardiovascular Imaging*, vol. 16, no. 7, pp. 723-730, 2015.
- [54] Vivitro Labs Inc. (2020, February) Vivitro Labs. [Online]. <https://vivotrolabs.com/product/pulse-duplicator/>
- [55] Vivitro Labs Inc. (2020, February) Vivitro Labs. [Online]. <https://vivotrolabs.com/product/endovascular-ev-simulator/>
- [56] Petrou A, Loepfe M, Yliruka M, Schumacher C.M., Kohll A.X., Starck C.T., Schmid Daners M, Meboldt M, Falk V, Stark W.J., Cohrs N.H., "A soft total artificial heart- first concept evaluation on a hybrid mock circulation," *Artificial Organs*, vol. 41, no. 10, pp. 948-958, 2017.
- [57] Science Direct. (2020, February) Science Direct. [Online]. <https://www.sciencedirect.com/topics/medicine-and-dentistry/heart-atrium-pressure>
- [58] Ultimaker. (2020, February) Ultimaker. [Online]. <https://ultimaker.com/download/74599/UM180821%20TDS%20PLA%20RB%20V10.pdf>
- [59] Ninjatek. (2020, February) Ninjatek. [Online]. <https://ninjatek.com/wp-content/uploads/2019/10/NinjaFlex-TDS.pdf>
- [60] Heart Valve Surgery. (2020, March) Heart Valve Surgery. [Online]. <https://www.heart-valve-surgery.com/heart-surgery-blog/2007/10/04/how-long-does-a-mechanical-mitral-valve-last/>
- [61] Heart Valve Surgery. (2020, March) Heart Valve Surgery. [Online]. <https://www.heart-valve-surgery.com/heart-surgery-blog/2007/12/19/biocore-aortic-valve-from-st-jude-medical/>

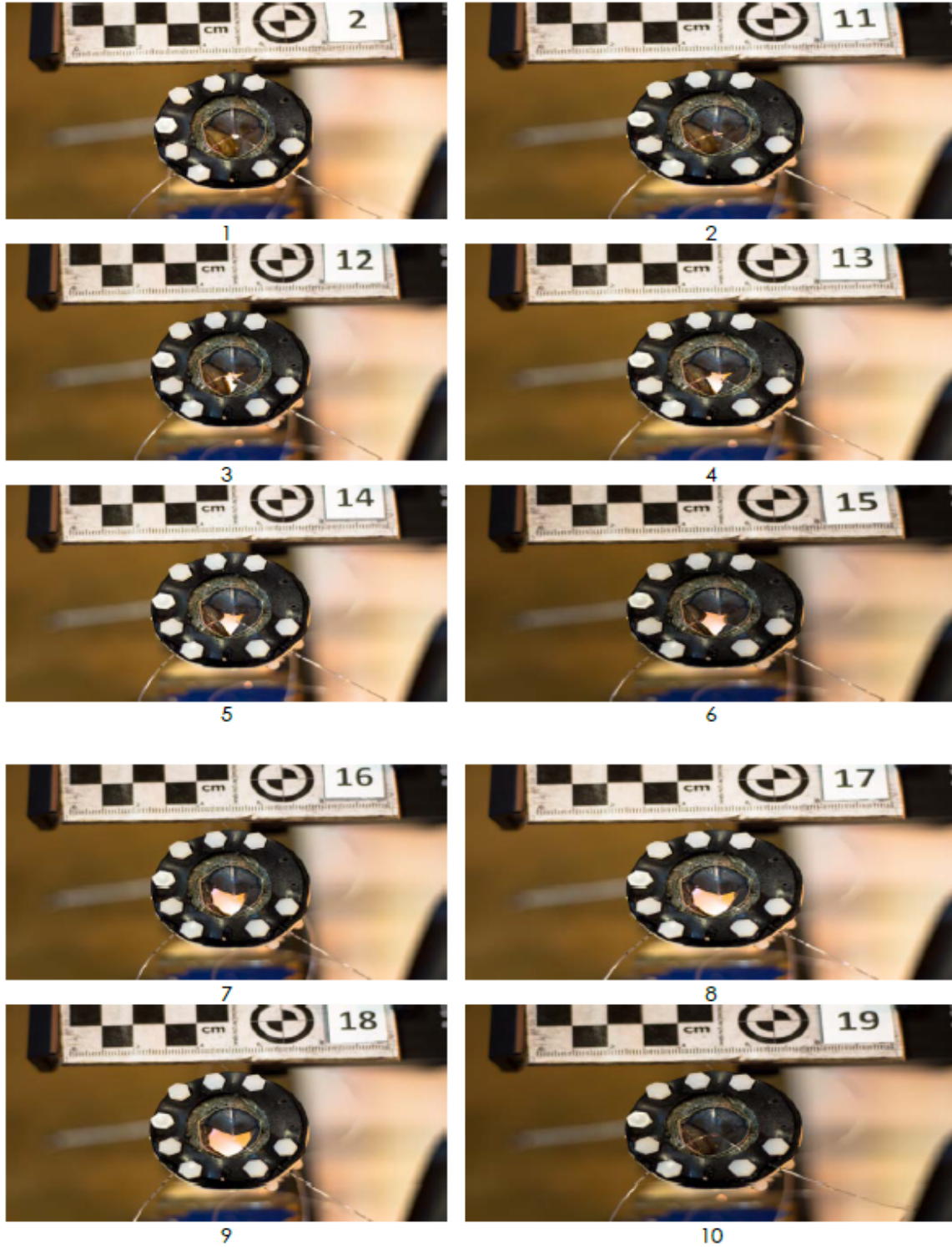
- [62] Lifelike Biotissue. (2020, March) Lifelike Biotissue. [Online]. <https://lifelikebiotissue.com/shop/cardiac-surgery/mitral-valve>
- [63] Schaff H.V., Morris J.J., Anderson B.J., Kopecky S.L., Enrique-Sarano M, Handa N, "Outcome of valve repair and the Cox maze procedure for mitral regurgitation and associated atrial fibrillation," *The Journal of Thoracic and Cardiovascular Surgery*, vol. 118, no. 4, pp. 628-635, 1999.
- [64] Schoepfoerster R, Dellsperger K.C., Chandran K.B., "Effect of prosthetic mitral valve geometry and orientation on flow dynamics in a model human left ventricle," *Journal of Biomechanics*, vol. 22, no. 1, pp. 51-65, 1989.
- [65] Ridgway J.P., "Cardiovascular magnetic resonance physics for clinicians: Part 1," *Journal of Cardiovascular Magnetic Resonance*, vol. 12, no. 1, p. 71, 2010.
- [66] Radiology Key. (2020, February) Radiology Key. [Online]. <https://radiologykey.com/mri-safety-2/>
- [67] Westbrook C, Talbot J, *M.R.I. in Practice*. Hoboken, NJ: John Wiley and Sons, 2018.
- [68] Radjenovic A, Ridgway J.P., Biglands J.D., "Cardiovascular magnetic resonance physics for clinicians: Part 2," *Journal of Cardiovascular Magnetic Resonance*, vol. 14, no. 1, p. 66, 2012.
- [69] Hassanabad A.F., François C.J., Garcia J, Jamalidinan F, "Four-dimensional-flow Magnetic Resonance Imaging of the Aortic Valve and Thoracic Aorta," *Radiologic Clinics*, vol. 58, no. 4, pp. 753-763, 2020.
- [70] Barker A.J., Markl M, Garcia J, "The role of imaging of flow patterns by 4D flow M.R.I. in aortic stenosis," *JACC: Cardiovascular Imaging*, vol. 12, no. 2, pp. 252-266, 2019.
- [71] Bissell M, Barker A.J., Bolger A.F., Carlhäll C.J., Ebbers T, Francios C.J., Frydrychowicz A, Geiger J, Giese D, Hope M.D., Dyverfeldt P, "4D flow cardiovascular magnetic consensus statement," *Journal of Cardiovascular Magnetic Resonance*, vol. 17, no. 1, p. 72, 2015.
- [72] Constantin C, Klersy C, Serio A, Fontana A, Campana C, Tavazzi L, Ghio S, "Interventricular and intraventricular dyssynchrony are common in heart failure patients, regardless of QRS duration ," *European Heart Journal*, vol. 25, no. 7, pp. 571-578, 2004.
- [73] Beppu S, Takahara Y, Nakajima N, Tanaka K, Ichihashi K, Fujita T, Manabe H, Kawazoe K, "Surgical treatment of giant left atrium combined with mitral valvular disease: Plication procedure for reduction of compression to the left ventricle, bronchus, and pulmonary parenchyma," *The Journal of Thoracic and Cardiovascular Surgery*, vol. 85, no. 6, pp. 885-

892, 1983.

- [74] Soft robotics toolkit. (2020, February) Soft robotics toolkit. [Online].
<https://softroboticstoolkit.com/book/case-study-cardiac-simulator>
- [75] Kuznetsov S.L., Froemming G.R.A., Muid S, Nor-Ashikin M.N.K., Otman S, Shahir A.R.M., Nawawi H, Kapitonova M.Y., "Effects of space mission factors on the morphology and function of endothelial cells," *Bulletin of Experimental Biology and Medicine*, vol. 154, no. 6, pp. 796-801, 2013.
- [76] Zhang H, Wang Z, Aydar M, Kitai T, Krittanawong C, "Artificial intelligence in precision cardiovascular medicine," *Journal of the American College of Cardiology*, vol. 69, no. 21, pp. 2657-2664, 2017.
- [77] newswise. (2020, May) newswise. [Online]
<https://www.newswise.com/institutions/view/1449>

Appendix

Appendix 1 Aortic Regurgitation Setup Selections



Appendix 2 Supervisor Information

Dr. Lyes Kadem, ing
users.encs.concordia.ca/~kadem
Laboratory of Cardiovascular Fluid Dynamics
Dept. Mechanical, Industrial and Aerospace Engineering
Concordia University



Julio Garcia, PhD, SNI-I, Junior FISMRM, SMIEEE
Assistant Professor
Libin Cardiovascular Institute - Stephenson Cardiac Imaging Centre
Alberta Children's Hospital Research Institute
Department of Radiology and Cardiac Sciences
University of Calgary - Cumming School of Medicine
SSB 0700, 1403 - 29 Street NW
Calgary, AB, Canada, T2N 2T9
T. (403) 944-2847

julio.garciaflores@ucalgary.ca
www.ucalgary.ca
<https://cumming.ucalgary.ca/labs/cadi>

Appendix 3 The MaxTron System



Appendix 4 System Maintenance

The system was designed to have as little maintenance as possible. A few important strategies have been implemented to ensure longevity of the system. The linear motor can benefit from regular greasing at intervals of approximately 30000 cycles. The circulatory system including reservoirs, tubing and heart components can occasionally be rinsed thoroughly with vinegar and water to eliminate the chance for fungicidal build up.

Disadvantages of the system are minimal and include regular small procedures to ensure proper functionality. The medical syringes used in the hydraulic activation system always need to be prepared back into motion slowly if they have been without use for more than one day and this inconsistency could easily be improved through further iterations of design changes. The biological heart valves need to be removed from the system and placed in water when the system is drained between uses in order to maintain the flexibility of the leaflets. To increase the lifespan of all 3D printed components, it is best to minimize the amount of loading they carry when the system is not being used which involves emptying all fluid from the system at the end of operations. Heat can be a serious threat to the system because 3D printed components tend to shrink when subjected to elevated temperatures. The repetitive action performed on the ventricles can cause them to wear thin which is cause for regular observation. The torso should be handled with care when being mobilized because solid 3D printed components along with the fiberglass mannequin torso are brittle.

Appendix 5 Experimentation Iterations

Primary results of pressure waveforms were far from accurate and the reason was because the set up at the time of these readings had no capillary resistance in the form of valves along the exit or return flow pathways. The Pulmonary Artery would branch off into two separate paths that were followed by soft rubber tubing with 1/2 inch inner diameter and 1/8 inch thickness. This was changed for the next iteration because it was believed to be the issue of why the pressure waves were different then the target waveforms. Another factor that played an important role towards achieving better

pressure waveforms was the fact that the opacity of the 3D printed heart components made it very hard to rid the system of all air bubbles which compromise the pressure reading accuracy. The results for the left ventricle pressure readings would show a dip in the waveform at the peak of the wave which is directly related to the air bubbles that were trapped in the system. With the previous silicone heart components it would be easier to locate and rid the system of all the air bubbles thanks to the transparency of the components. After a few attempts, an adequate procedure of placing the system to relieve all the trapped air was found and pressure readings slowly became more acceptable. Pressure waveforms obtained from the right ventricle showed that changing the exit tubing of the pulmonary artery for more flexible tubes was beneficial for decreasing the amplitude of the waveform which was close to 70 mmHg and should have been near 25. A solution for more flexible tubing was found in the form of long birthday balloons which offered the ultimate elasticity that was readily available to the general public. The system was updated with an extra set of hydraulic pushers that would act upon the atriums. When the right ventricle would begin its systolic cycle, which is when the ventricle is filled with fluid, the linear motor would be in retraction pulling the pusher off the ventricle allowing it to fill itself up with gravity potential from the elevated reservoir. The second hydraulic system was attached to the returning end of the linear motor meaning that it would push and activate the right atrium while the right ventricle was filling up. Since the right atrium empties into the right ventricle, the pushers helped the filling process. When the pusher of the ventricle would activate and apply pressure on the ventricle, the return stroke of the atrium pusher was relieved allowing the atrium to refill itself from the reservoir directly. The use of the secondary hydraulic system was

proven effective and added to the realism of the simulation but was not developed further due to the force budget that the linear motor was capable of.

Different methods were attempted where either squeezing was performed on tube sections at different locations or the tubes were placed at different elevations to calibrate the pressure readings. The good thing that came from this trial was that the waveforms were looking more like the target waveforms of a healthy heart. However, the disadvantage was that results were difficult to reproduce since the means in obtaining them were very specific and not measurable through that approach. Another important factor that helped the stabilization of the pressure readings was the extra support added to the heart support structure. The vibrations caused by the loose components really hindered the progress of the research and once dealt with relieved the results from non-physiological effects.

The left side, although rudimentary, represents an entirely different approach than previously attempted. The 3D printed aorta was replaced by a custom silicone component which adds the advantage of transparency for air bubble elimination and recreates the medical training simulation of transcatheter procedures more accurately than rubber tubing.



Concordia
M O N T R É A L

[77]